Title: Coordination between ECM and cell-cell adhesion regulates the development of islet aggregation, architecture, and functional maturation

Wilma Tixi[1, 7], Maricela Maldonado[1, 7], Ya-Ting Chang[1, 7], Amy Chiu[1], Wilson Yeung[1], Nazia Parveen[1], Michael Nelson[2], Ryan Hart[3], Shihao Wang[4], Wu Jih Hsu[4], Patrick Fueger[5] Janel L. Kopp[4], Mark O. Huising[3, 6], Sangeeta Dhawan[1], and Hung-Ping Shih[1, *]

[1] Department of Translational Research and Cellular Therapeutics, Arthur Riggs Diabetes and Metabolic Research Institute, Beckman Research Institute, City of Hope, Duarte, CA, USA

[2] Light Microscopy Core, Beckman Research Institute, City of Hope, Duarte, CA, USA

[3] Department of Neurobiology, Physiology and Behavior, College of Biological Sciences, University of California, Davis, Davis, CA, USA

[4] Department of Cellular and Physiological Sciences, Life Sciences Institute, University of British Columbia, Vancouver, British Columbia, Canada

[5] Department of Molecular & Cellular Endocrinology, Arthur Riggs Diabetes and Metabolic Research Institute, Beckman Research Institute, City of Hope, Duarte, CA, USA

[6] Department of Physiology and Membrane Biology, School of Medicine, University of California, Davis, Davis, CA, USA

[7] These authors contributed equally to this work.

[*]Corresponding author: hshih@coh.org

HIGHLIGHTS

- Islet vascularization and aggregation are regulated via ECM-Itgb1 signaling
- ECM-Itgb1 signaling negatively controls islet aggregation via regulation of cell-cell adhesion during development
- Cell-cell adhesion negatively regulates the interaction of endocrine cell-vasculature in islets
- Differential cell adhesion regulates the establishment of islet architecture
- Endocrine functional maturation depends on islet aggregation regulated by the coordination of ECM-Itgb1 signaling and cell-cell adhesion

SUMMARY

Pancreatic islets are 3-dimensional cell aggregates consisting of unique cellular composition, cell-to-cell contacts, and interactions with blood vessels. Cell aggregation is essential for islet endocrine function; however, it remains unclear how developing islets establish aggregation. By combining genetic animal models, imaging tools, and gene expression profiling, we demonstrate that islet aggregation is regulated by extracellular matrix signaling and cell-cell adhesion. Islet endocrine cell-specific inactivation of extracellular matrix receptor Integrin β1 disrupted blood vessel interactions but promoted cell-cell adhesion and the formation of larger islets. In contrast, ablation of cell-cell adhesion molecule α-Catenin promoted blood vessel interactions yet compromised islet clustering. Simultaneous removal of Integrin β1 and α-Catenin disrupts islet aggregation and the endocrine cell maturation process, demonstrating that establishment of islet aggregates is essential for functional maturation. Our study provides new insights into understanding the fundamental self-organizing mechanism for islet aggregation, architecture, and functional maturation.

INTRODUCTION

To control various physiological responses, groups of endocrine cells cluster together with vasculature, mesenchymal cells, and neuronal cells to form a highly organized "mini-organ" in the pancreatic epithelium: the islet of Langerhans. The islet endocrine cells emerge from a domain of multipotent progenitors in the embryonic pancreatic epithelium. Initially, the multipotent pancreatic progenitors resolve into a pre-acinar domain, and a bipotential endocrine/ductal progenitor domain of the developing pancreas (Larsen and Grapin-Botton, 2017; Romer and Sussel, 2015; Shih et al., 2013). Endocrine cell progenitors are specified by the expression of the pro-endocrine gene *Neurogenin 3* (*Ngn3*) (Gu et al., 2002). Following endocrine cell specification, the Ngn3$^+$ precursors undergo delamination (Bechard et al., 2016; Gouzi et al., 2011; Rosenberg et al., 2010). Delaminated endocrine precursors remain associated with the ducts as they migrate and join other endocrine cells and aggregate into immature islets (Sharon et al., 2019a). These immature islets form long interconnected cords along the ductal epithelium. Later the islet cords change morphology and undergo fission to form distinct spherical islets (Jo et al., 2011; Seymour et al., 2004; Sznurkowska et al., 2020). Throughout the differentiation and morphological changes, endocrine cells are intimately associated with the vasculature, which facilitates functional control of hormone release (Reinert et al., 2014). To coordinate the hormone release of endocrine cells within each islet, autocrine and paracrine interactions, as well as direct cell contacts are required (Campbell and Newgard, 2021). These interactions are established by the aggregation process during development (Adams and Blum, 2022). Defects in the aggregation processes may lead to defects in endocrine cell development, and eventually, islet dysfunction. Supporting this notion, human pluripotent stem cell (hPSC)-derived β-cells acquire more functional maturity *in vitro* if clustered together (Cottle et al., 2021; Nair et al., 2019). However, the mechanism by which this process is regulated *in vivo* has largely remained elusive.

Self-organization of a group of cells into a higher-order, multicellular functional unit relies on an array of cell interactions regulated by cell-cell adhesions (Fagotto, 2014). For example, a calcium-dependent adhesion molecule, Neural Cell Adhesion Molecule (N-CAM), has been shown to be critical for murine endocrine cells to cluster (Esni et al., 1999). In rodents, islets form a stereotypical core-mantle architecture in which the Insulin (Ins) secreting β-cells are located mainly in the central core, with Glucagon (Gcg) secreting α-cells and Somatostatin (Sst) secreting δ-cells localizing in the periphery to form a mantle (Adams and Blum, 2022; Arrojo e Drigo et al., 2015; Kim et al., 2009). In culture, dissociated rat endocrine cells can self-organize into the core–mantle architecture, suggesting that the islet structure is established by factors intrinsic to endocrine cells (Halban et al., 1987). N-CAM deleted mice show abnormal islet architecture, with α-cells spread throughout the islet core and abnormal assembly of adherens junction proteins N- and E-cadherin (Ncad and Ecad) (Esni et al., 1999). In addition, ectopic expression of a dominant negative Ecad in mouse β-cells interferes with their clustering and islet formation (Dahl et al., 1996); and loss of *Ecad* results in abnormal blood glucose homeostasis (Wakae-Takada et al., 2013). Intracellularly, adherens junctions are stabilized by β-Catenin (*Ctnnb1*) and α-Catenin (*Ctnna1*) (Jamora and Fuchs, 2002). The function of *Ctnnb1* has been extensively studied in the developing pancreas (Elghazi et al., 2012; Murtaugh et al., 2005; Rulifson et al., 2007) and in hPSC-derived β-cells, because of its role in cell proliferation via Wnt signaling (Sharon et al.,

2019b); yet genetic studies show that *Ctnnb1* is not essential for islet clustering and architecture (Elghazi et al., 2012; Murtaugh et al., 2005). In the developing pancreas, inactivation of *Ctnna1* results in defects in endocrine progenitor differentiation due to an expansion of pancreatic ductal progenitors (Jimenez-Caliani et al., 2017). Whether the process of islet clustering and architecture requires *Ctnna1* is unknown.

The regulation of cell-cell adhesion is often coupled with cell-extracellular matrix (ECM) interaction and Integrin signaling (Mui et al., 2016; Weber et al., 2011). Upon ECM binding, Integrins activate signal transduction pathways and regulate 1) cytoskeleton dynamics, 2) cell movement, 3) cell differentiation, and 4) functional maturation of epithelial cells, vasculature, and neurons (Barros et al., 2011; Li et al., 2008; Scheppke et al., 2012). During angiogenesis, ECM receptor Integrin β1 (Itgb1) is required to control the localization of cell-cell adhesion molecule VE-cadherin and maintain cell–cell junction integrity (Yamamoto et al., 2015). In salivary glands and early embryonic pancreas, Integrin β1-mediated ECM adhesions regulate Ecad to control cell clustering and regulate budding epithelial branching (Shih et al., 2016; Wang et al., 2021; Wang et al., 2017). Whether islet morphogenesis also requires ECM-Integrin signaling remains to be investigated.

In the present study, we examine how loss of *Itgb1* and *Ctnna1* in Ngn3-expressing endocrine progenitors affects islet morphogenesis. We show that *Itgb1* and *Ctnna1* have collaborative roles during islet aggregation: ECM-Itgb1 signaling modulates islet aggregation by negatively regulating cell-cell adhesions; and α-Catenin promotes endocrine cell clustering and modulates vascularization during islet development. We also provide evidence that the islet architecture is regulated by differential adhesion in endocrine subtypes.

RESULTS

The morphogenesis and functional maturation of islet endocrine cells depend on ECM-Itgb1 signaling during development.

To investigate the process of islet aggregation, embryonic day 15.5 (E15.5) pancreas was stained for blood vessel maker PECAM, ductal marker Spp1, and endocrine cell marker Chromogranin A. Confocal microscopy and 3D whole-mount immunofluorescence imaging revealed that at E15.5 endocrine cells had started aggregating, and the vascular and ductal networks were already highly similar (Figure S1A). This close relation between the ducts and blood vessels at the stage prior to islet aggregation suggests that blood vessels could readily interact and provide instructive cues to regulate endocrine progenitor aggregation into islets. Blood vessels in islets produce ECM-rich basal membrane to support and organize endocrine cells (Lammert et al., 2003; Roscioni et al., 2016). Thus, we hypothesized that ECM signaling, provided by the vasculature, plays a key role in the initiation steps of islet aggregation. Supporting this notion, published work using single-cell gene expression profiling shown that the ECM-Itgb1 signaling gene ontology (GO) categories are most significantly enriched in the Ngn3^{+} endocrine progenitors (Bastidas-Ponce et al., 2019). Immunofluorescence (IF) analysis validated that both the Ngn3^{+} endocrine progenitors and their progenies (eYFP^{+} cells in *Ngn3-Cre; Rosa26-eYFP* pancreas) expressed Itgb1 (Figure 1A). To investigate the role of Itgb1 during endocrine cell aggregation, we used the *Ngn3-Cre* allele to recombine the *Itgb1-flox* alleles in endocrine progenitors (*Ngn3-Cre*; *Itgb1$^{f/f}$*;

142 hereafter *Itgb1*$^{\Delta Endo/\Delta Endo}$). Expression of Itgb1 was almost entirely absent throughout the islet
143 endocrine cells in comparison to control littermates at 6 weeks old (Figure 1B,1C). We first
144 examined whether inactivation of ECM-Itgb1 signaling affected vascular interaction. Electron
145 microscope ultrastructure analysis revealed tight attachment in basal membranes between
146 vascular and endocrine cells in control islets (Figure S1B). In contrast, in the *Itgb1*$^{\Delta Endo/\Delta Endo}$ islets,
147 the endocrine cells were detached from the basal membranes of blood vessels (Figure S1C, red
148 arrows). Despite the vascular defects with Itgb1 loss, all four endocrine cell subtypes, α-, β-, δ-,
149 and Ppy- (pancreatic polypeptide) cells, were present at similar proportions in control and
150 *Itgb1*$^{\Delta Endo/\Delta Endo}$ islets (Figure 1D,1E;S1D-S1G). In addition, the expression of β-cell lineage
151 markers Nkx6.1 and Pdx1 were present in the Ins^{+} cells of control and *Itgb1*$^{\Delta Endo/\Delta Endo}$ islets (Figure
152 1F,1G). Although the populations of endocrine cell lineages were unaffected by the loss of *Itgb1*,
153 morphometrical analysis revealed drastic morphological changes. In control islets, β-cells were
154 organized in a central core and surrounded by α- and δ- cells in the periphery (Figure 1D).
155 Conversely, in *Itgb1*$^{\Delta Endo/\Delta Endo}$ mice, several individual islets appeared to agglomerate, resulting in
156 larger islet sizes and aberrant distribution of α- and δ- cells in the central core (Figure 1E,1G; S1I).
157 Thus, the inactivation of Itgb1 has a profound impact on islet morphogenesis, but not endocrine
158 cell fate choice.

159 We next investigated whether the loss of *Itgb1* had any impact on the expression of genes related
160 to islet function. Islets from 6 weeks old control and *Itgb1*$^{\Delta Endo/\Delta Endo}$ mice were isolated and
161 subjected to RNA-seq and differential gene expression analysis. A comparison of gene-
162 expression profiles between *Itgb1*$^{\Delta Endo/\Delta Endo}$ and control islets revealed 417 differentially
163 expressed genes (DEGs) with false discovery rate (FDR) < 0.05 and fold change (FC)>2 (Table
164 S1), of which 332 were up-regulated and 85 were down-regulated. Gene-set enrichment analysis
165 (GSEA) of DEGs between control and *Itgb1*$^{\Delta Endo/\Delta Endo}$ islets showed up-regulation of pathways
166 associated with hypoxia, epithelial mesenchymal transition, glycolysis, and inflammatory
167 response (Figure 1H). The analysis of Gene Ontology (GO) of Differentially Expressed Genes
168 (DEGs) related to hypoxia showed that the genes responsible for hypoxia response were up-
169 regulated in *Itgb1*$^{\Delta Endo/\Delta Endo}$ islets when compared to the control group (as shown in Figure S1L).
170 The immunofluorescence (IF) analysis indicated that the *Itgb1*$^{\Delta Endo/\Delta Endo}$ islets at 2-3 months old
171 displayed a significant reduction in blood vessels (as shown in Figure S1M-S1O), which suggests
172 that the lack of vascular interaction could lead to hypoxia responses. On the other hand, the down-
173 regulated genes were associated with spermatogenesis, pancreas β-cells, and E2F targets
174 (Figure 1H). GO analysis of DEGs in the pancreas β-cells category further revealed that functional
175 maturation genes for β-cells (e.g., *Slc2a2* (*Glut2*), *Ucn3*, and *Mafa*) and for α-cells (e.g., *Arx*, *Mafb*,
176 and *Etv1*), were drastically down-regulated in the *Itgb1*$^{\Delta Endo/\Delta Endo}$ islets (Figure 1I, Group 1, S2A).
177 IF analysis also validated the reduced expression of Mafa, Ucn3, and Glut2 in β-cells of
178 *Itgb1*$^{\Delta Endo/\Delta endo}$ islets (Figure S2B-E). Furthermore, several "disallowed" genes for β-cells,
179 including *Ldha1*, *Aldh1a3*, and *Hk1* (Lemaire et al., 2016), were significantly up-regulated in the
180 *Itgb1*$^{\Delta Endo/\Delta Endo}$ islets (Figure 1I, Group 2, S2A). Hence, it is likely that the functional maturation of
181 endocrine cells within *Itgb1*$^{\Delta Endo/\Delta Endo}$ islets is compromised. This notion is supported by the
182 observation that, by 6 weeks of age, these mice exhibit glucose intolerance and reduced insulin
183 secretion in response to glucose stimulation (Figure 1J-K). The impairment in glycemic regulation
184 further deteriorates in mice older than 6 months (Figure 1L). Together, these observations indicate

185 that ECM-integrin interactions are critical for islet vascularization, morphogenesis, and the
186 functional maturation of endocrine cells.

187 *ECM signaling regulates endocrine progenitor cell migration and cell-cell adhesion to control islet*
188 *aggregation during development.*
189 Our initial analysis of the pancreatic sections from *Itgb1*$^{\Delta Endo/\Delta Endo}$ mice revealed larger islet sizes
190 (Figure S1J). Consistently, the islets isolated from *Itgb1*$^{\Delta Endo/\Delta Endo}$ mice appeared larger in size as
191 well (Figure 2A-2C); however, the total islet area was similar between control and *Itgb1*$^{\Delta Endo/\Delta Endo}$
192 mice (Figure 2D). The increased size was mainly attributed to a greater number of large islets
193 (>50 μm^2 x 10^3, as shown in Figure S1K,2E). Therefore, the enlarged islet size is likely a result of
194 a morphological change independent of the expansion of total endocrine cells. Furthermore, in
195 the control pancreata, the islets were located near the ducts, but contained a very small number
196 of ductal cells (Figure 2F,2H,S3A). In contrast, the islets in the *Itgb1*$^{\Delta Endo/\Delta Endo}$ pancreata contained
197 a substantial number of ductal cells (Figure 2G,2H,S3B). As the endocrine progenitors arise and
198 migrate away from the ducts, we hypothesized that there might be deficiencies in this process for
199 Itgb1-deficient endocrine cells. To investigate this, we conducted segmentation analysis of 3D
200 whole-mount immunofluorescence on E15.5 pancreata, the stage at which the majority of
201 endocrine progenitor migration occurs (Rosenberg et al., 2010). Our results showed that most of
202 the Itgb1-deleted endocrine progenitor cell aggregates had a greater tendency to cluster within
203 the ductal cords during development (Figure 2I,2J and Movie S1; the green color represents zero
204 distance from ducts). These findings imply that there might be deficiencies in both endocrine cell
205 migration and premature islet aggregation in *Itgb1*-deleted endocrine cells. To further confirm this,
206 we conducted live-imaging analysis on pancreas explants obtained from E16.5 *Ngn3-Cre;*
207 *R26mT/mG; Itgb1*$^{+/+}$ (control) and *Ngn3-Cre; R26mT/mG; Itgb1*$^{f/f}$ (*Itgb1*$^{\Delta Endo/\Delta Endo}$) mice. We
208 tracked the movement and aggregation of Ngn3-progeny (mGFP$^+$) endocrine progenitor cells in
209 explant cultures for up to 3 days (Figure S3C,S3D; Movie S2,S3). Our observations showed that
210 in contrast to the controls, where endocrine progenitor cells migrated and aggregated outside of
211 ductal cords, the mGFP$^+$ cells in *Itgb1*$^{\Delta Endo/\Delta Endo}$ explants readily aggregated before moving away
212 from the cords (Figure S3D white arrows). In contrast to our findings, previous studies using *Ins-*
213 *Cre* or *RIP-Cre* to ablate *Itgb1* after endocrine progenitors have differentiated into insulin-
214 producing cells did not report any observable islet aggregation or migration defects (Diaferia et
215 al., 2013; Win et al., 2020). However, *Ngn3-Cre* mediated *Itgb1* deletion would occur much earlier
216 in embryonic stages (Figure 1A), suggesting that Itgb1 signaling regulates the migration and
217 aggregation of progenitor cells in the endocrine lineage during the islet developmental process.
218
219 To further investigate this notion, we sought to inactivate Itgb1 only after the endocrine cells had
220 fully differentiated and matured. Urocortin 3 (Ucn3) is a late β-cell-specific maturity marker in
221 mouse islets that is expressed after *Ins1* and *Ins2* and starts perinatally. Most β-cells express
222 Ucn3 by 3 weeks of age (Blum et al., 2014; van der Meulen and Huising, 2014). The expression
223 pattern of Cre recombinase under the control of the *Ucn3* promoter aligns with this timeline (van
224 der Meulen et al., 2017). Therefore, *Ucn3-Cre* mediated deletion of *Itgb1* is not expected to occur
225 until islet development has completed in the presence of functional Itgb1 alleles and normal Itgb1
226 expression. To test whether Itgb1 signaling also maintains islet cell aggregation after β-cell
227 maturation and islet formation, we crossed *Ucn3-Cre* with *Itgb1*$^{f/f}$ mice to inactivate Itgb1

228 exclusively in mature β-cells (referred to as *Itgb1*$^{\Delta Mature\beta/\Delta Mature\beta}$). Our analysis revealed that, similar
229 to *Itgb1*$^{\Delta Endo/\Delta Endo}$ mice, *Itgb1*$^{\Delta Mature\beta/\Delta Mature\beta}$ mice exhibited vasculature exclusion from islets (Figure
230 S3E',S3F'), but their islet size remained similar to control mice (Figure S3E-S3I). These results
231 suggest that Itgb1 signaling specifically regulates islet cell aggregation during pancreatic
232 development.
233
234 During the early stages of pancreas development, the expression of Itgb1 in pancreatic progenitor
235 cells has been identified as a crucial factor in controlling pancreas branching morphogenesis
236 through its regulation of cell-cell adhesion (Shih et al., 2016). As the process of endocrine
237 progenitor cell differentiation and islet formation commences, cell-cell adhesion is typically
238 downregulated to facilitate the migration and interaction of endocrine cells with non-endocrine
239 cells (Gouzi et al., 2011). Given the established role of Itgb1 in regulating cell-cell adhesion in the
240 context of pancreas development, we were prompted to investigate whether Itgb1 signaling also
241 plays a role in instructing endocrine progenitor cells to modulate their adhesion behavior and
242 thereby control the islet aggregation process. To address this question, we took Airyscan super-
243 resolution images of Ecad IF on endocrine cells in *Ngn3-Cre; R26mT/mG; Itgb1*$^{f/f}$ islets at P7,
244 since islet aggregation is complete by the neonatal stages (Sznurkowska et al., 2020). The
245 Airyscan images provide sufficient resolution to show adherens junctions between cells by
246 visualizing Ecad^{+} clusters ((Gonschior et al., 2020); white dots in Figure 2K,2L). The lineage-
247 traced endocrine cells (mGFP^{+}) in control islets displayed low amounts of Ecad^{+} clusters (Figure
248 2K'). However, the amount of Ecad^{+} clusters was drastically increased in mutant islets (Figure
249 2L'), suggesting that Itgb1 signaling negatively regulates cell adhesion in developing islets. To
250 further test whether the increased cell adhesiveness is responsible for the increased islet size
251 when Itgb1 signaling is disrupted, we performed an *in vitro* cell aggregation assay. Live mGFP^{+}
252 endocrine cells, from neonatal (P2-P4) *Ngn3-Cre; R26mT/mG; Itgb1*$^{+/f}$ or *Ngn3-Cre; R26mT/mG;*
253 *Itgb1*$^{f/f}$ pancreata, were completely dissociated, then collected by FACS. 3000 mGFP^{+} cells were
254 allowed to aggregate in wells of a 96-well plate that were coated with bovine serum albumin (no
255 ECM) or Matrigel and fibronectin (+ECM) (Figure 2M). Within 2 hours of cell seeding, the control
256 mGFP^{+} endocrine cells rapidly aggregated in wells with no ECM coating, but formed no
257 aggregates in the ECM-coated wells (Figure 2N-2P). Within the same amount of time, the mutant
258 mGFP^{+} endocrine cells clustered into larger aggregates in wells without ECM coating and
259 maintained aggregation in the ECM-coated wells (Figure 2N,2Q,2R). After 48 hours, the mGFP^{+}
260 cells isolated from both the controls and mutants progressively clustered into larger aggregates
261 in wells without ECM coating (Figure S4A-S4C,S4E). In contrast, in the ECM-coated wells, only
262 the mutant mGFP^{+} cells clustered, while control mGFP^{+} cells remained unaggregated (Figure
263 S4D,S4F). Together, these findings demonstrated that ECM-Itgb1 signaling negatively regulates
264 islet aggregation. As Integrins play a crucial role in linking the actin cytoskeleton, we examined
265 whether the inactivation of Itgb1 in endocrine progenitors affects the organization of the actin
266 cytoskeleton in islet cells. In *Itgb1*$^{\Delta Endo/\Delta Endo}$ islets, we observed pronounced foci of condensed F-
267 actin between the endocrine cells (Figure S4G-S4J), indicating increased cell-cell adhesion.
268 These findings suggest that the loss of Itgb1 in endocrine cells leads to alterations in the actin
269 cytoskeleton, resulting in enhanced cell-cell adhesion within the islet microenvironment. The
270 concentrated F-actin foci between the endocrine cells indicate a potential mechanism through
271 which Itgb1 regulates cell-cell interactions and influences islet development and aggregation.

α-Catenin promotes endocrine cell aggregation and regulates vascularization during islet development.

Our study revealed that Itgb1 plays a critical role in islet development by regulating endocrine cell-cell adhesion. However, the mechanism by which cell-cell adhesion regulates islet formation remains unclear. Although Ecad and Ncad-mediated adherens junctions are believed to be the primary cell-cell adhesion mechanisms linking islet cells into aggregates, our findings and other studies have shown that deletions of Ecad or Ncad alone do not affect islet aggregation, suggesting functional redundancy between these cell adhesion molecules.

α-Catenin (Ctnna1) is an essential hub protein linking Ecad-mediated adherens junctions to the cytoskeleton and has been demonstrated to be indispensable for the formation of adherens junctions(Jamora and Fuchs, 2002). Therefore, to investigate the requirement of cell adhesion in islet formation, we conditionally ablated Ctnna1 in endocrine progenitors by generating *Ngn3-Cre*; *Ctnna1*$^{f/f}$ mice (hereafter referred to as *Ctnna1*$^{\Delta Endo/\Delta Endo}$). To determine whether *Ctnna1* deletion affects islet development, Chromogranin A (ChrA) staining on pancreas sections from 8 weeks old mice were imaged, and the total relative islet area was measured (Figure 3A,3B). Compared to their wild-type littermates, islet area (relative to the total pancreas area) in *Ctnna1*$^{\Delta Endo/\Delta Endo}$ mice was unchanged (Figure 3C), but there was a significant reduction in average islet size (Figure 3D). The proportion of larger islets was significantly reduced, while the proportion of small islets was increased (Figure S5A-S5C), suggesting that *Ctnna1* is required for proper islet aggregation, but not for the development of total islet cell mass. In *Ctnna1*$^{\Delta Endo/\Delta Endo}$ islets, we observe diminished Ecad expression and a decrease in the density of F-actin at cell junctions. These findings imply a disruption of cell junctions and a reduction in cell adhesion among Ctnna1-deficient endocrine cells (Figure 3E, 3F).

To investigate how *Ctnna1*-deletion impacts islet development, we compared transcriptional profiling of *Ctnna1*$^{\Delta Endo/\Delta Endo}$ and control islets at 8 weeks. A comparison of gene expression profiles between *Ctnna1*$^{\Delta Endo/\Delta Endo}$ and control islets revealed significant differences in the expression of 319 genes with FDR < 0.05 and FC>2, of which 245 were up-regulated and 74 were down-regulated (Table S2). Among all GO categories, one of the most up-regulated groups in *Ctnna1*$^{\Delta Endo/\Delta Endo}$ islets is genes associated with ECM signaling and blood vessel interactions (Figure 3G, S5D). These include Metalloproteases, Vascular Adhesion, Collagens, Integrins, Laminins, Glycoproteins and Thrombospondins (Figure 3G). These findings suggested that *Ctnna1*$^{\Delta Endo/\Delta Endo}$ islets have augmented ECM signaling and blood vessel interaction. IF for blood vessels confirmed an increase in blood vessel density in *Ctnna1*$^{\Delta Endo/\Delta Endo}$ islets at 8 weeks (Figure 3H-3J). The increase in islet vasculature was observed as early as P14 (Figure 3K-3L). These findings demonstrated that the inactivation of *Ctnna1* in endocrine progenitor cells led to a decrease of endocrine cell-cell adhesion and an increase in blood vessel interaction.

Alongside the increased interaction with blood vessels, we observed abnormal organization of F-actin fibers within *Ctnna1*$^{\Delta Endo/\Delta Endo}$ islets (Figure 3E, 3F; S5E, S5F). These alterations in F-actin fiber organization were evident as early as P14 in the *Ctnna1*$^{\Delta Endo/\Delta Endo}$ islets, concurrent with the onset of enhanced interaction with blood vessels (Figure S5G, S5H). These findings demonstrate that the loss of Ctnna1 compromises endocrine cell aggregation and perturbs the

organization of the actin cytoskeleton and cell-cell adhesion. Together, these findings suggest that the balance between cell-cell adhesion and blood vessel interaction is crucial for islet cell aggregation during development (Figure S5I).

Inactivation of Ctnna1 in differentiating endocrine cells affects the assembly and maintenance of non-β endocrine cells in islets.

To further investigate the impact of Ctnna1-dependent islet cell aggregation on the islet development process, we compared the gene expression profiles of *Ctnna1*$^{\Delta Endo/\Delta Endo}$ and control islets. Our analysis revealed significant misregulation of genes crucial for endocrine cell functions. Specifically, we observed a down-regulation of *Slc27a2*, *Tmsb15b1*, and *Etv1* expression, which are genes required for glycemic control and insulin secretion (Figure 4A Group 1, S6A,). Conversely, we found an up-regulation of *Hk1*, *Ldha*, *Aldh1a1*, and *Cxcl14* expression, which are genes known to be "disallowed" in mature functional β-cells (Lemaire et al., 2016) (Figure 4A Group 2, S6A). These findings suggest that the function of β-cells may be negatively impacted in *Ctnna1*$^{\Delta Endo/\Delta Endo}$ mice.

To support this notion, we conducted glucose tolerance tests, which revealed mild glucose intolerance in *Ctnna1*$^{\Delta Endo/\Delta Endo}$ mice at 8 weeks (Figure 4B). However, the quantification of insulin content in serum after glucose challenge did not reveal any noticeable insulin secretion defect in the *Ctnna1*$^{\Delta Endo/\Delta Endo}$ mice (Figure 4C). We reasoned that the conventional serum insulin measurement may not reflect the changes in β-cell function, given that the *Ctnna1*$^{\Delta Endo/\Delta Endo}$ mice exhibit only mild glucose intolerance. Therefore, we performed quantification of insulin secretion *in vivo* using hyperglycemic clamps, which is a more sensitive detection method. In this assay, we observed a trend towards lower overall insulin secretion in the *Ctnna1*$^{\Delta Endo/\Delta Endo}$ mice at 8 weeks (Figure S6B,S6C), providing additional evidence that Ctnna1-dependent islet cell aggregation has an impact on β-cell function. In addition, the glucose intolerance phenotype became even more pronounced at one year of age, as evidenced by glucose tolerance test (Figure 4D). These findings indicate that Ctnna1-dependent islet cell aggregation is crucial for the proper development of β-cells and their function in maintaining glucose homeostasis.

In addition to suggested functional defects in β-cells, we found that genes for non-β endocrine cell lineages, including α-cell genes *Gcg, MafB, Arx, Peg10,* and *Etv1,* and the δ-cell gene *Sst*, were significantly down-regulated in *Ctnna1*$^{\Delta Endo/\Delta Endo}$ islets (Figure 4A; S6A,), suggesting the requirement of *Ctnna1* for the presence of non-β endocrine cells in islets. Interestingly, *Ctnna1*$^{\Delta Endo/\Delta Endo}$ islets did not show a reduced area of β-cells, as β-cells were still organized loosely in the core of islets (Figure 4E-4G). However, there was a severe reduction of α-cell and δ-cell populations in the *Ctnna1*-deleted islets (Figure 4H; S6D-S6F). To determine whether the loss of non-β endocrine cells was the result of differentiation defects during development, we examined the population of α- and β-cells in *Ctnna1*$^{\Delta Endo/\Delta Endo}$ islets at P0 and P7. At these ages, the islets of *Ctnna1*$^{\Delta Endo/\Delta Endo}$ mice exhibited normal endocrine cell mass, Gcg^{+} α-cell and Sst^{+} δ-cell areas (Figure 4I-4K; S6G-S6J), demonstrating that the loss of α- and δ-cell was not due to differentiation defects prior to these early stages. However, the detachment of α-cells from the mantle of *Ctnna1*$^{\Delta Endo/\Delta Endo}$ islets was observed by P7. By this time point, α-cells had formed tight interactions with other endocrine cells in control islets (Figure S6I,S6K), but *Ctnna1*-deficient α-

360 cells detached from other cell types (Figure S6J,S6L). To investigate whether cell detachment
361 promotes cell death, thus resulting in α-cell loss, TUNEL analysis on P7 *Ctnna1*$^{\Delta Endo/\Delta Endo}$ islets
362 was conducted to analyze cell apoptosis. Compared to the control, *Ctnna1*$^{\Delta Endo/\Delta Endo}$ islets display
363 3 times more TUNEL^{+} apoptotic α-cells (Figure 4L-4N), indicating that *Ctnna1* is required for α-
364 cell survival. Thus, the loss of the α-cells in *Ctnna1*$^{\Delta Endo/\Delta Endo}$ islets during adulthood is not due to
365 endocrine cell differentiation defects; instead, a drastic increase in apoptosis explains the loss of
366 α-cells in the *Ctnna1*-deleted islets.
367
368 *Differential adhesion in endocrine cells controls the formation of islet architecture.*
369 Since the reduction of cell-cell adhesion caused distinctive outcomes in different endocrine cell
370 subtypes, we hypothesized that the endocrine cells in the mantle or core of islets may have
371 different adhesiveness. We re-analyzed publicly available gene expression profiles (DiGruccio et
372 al., 2016) to examine the expression of key cell adhesion molecules *E-cadherin*, *N-cadherin*, *α-*
373 *Catenin*, and *β-Catenin* between the subtypes of endocrine cells. These adhesion genes were
374 expressed at the highest level in β-cells, while their expression was comparatively lower in
375 endocrine cells located in the mantle of islets (α-cells and δ-cells, Figure S7A). These
376 observations suggest that the adhesive properties may differ between endocrine cell subtypes.
377 According to the differential adhesion hypothesis (DAH), a population of cells with different
378 adhesive properties will tend to spontaneously sort themselves to maximize adhesive bonding
379 (Foty and Steinberg, 2005). Stronger adhesion between β-cells may lead to them bundling into
380 islet cores, while the weaker adhesion between non-β-cells results in their dispersion into islet
381 mantles.
382
383 Based on the DAH, if the cell adhesion is altered in different endocrine subpopulations, the
384 stereotypical islet architecture will also be affected. To alter the cell adhesion in different
385 endocrine subpopulations, we crossed *Ins1-Cre* and *Gcg-iCre* lines to *Ctnna1-flox* mice and
386 traced the *Ctnna1*-deleted β- or α-cells with the lineage tracer *Rosa26-mT/mG* (*Ins1-Cre*; *Ctnna1*$^{f/f}$;
387 *Rosa26-mT/mG* and *Gcg-iCre; Ctnna1*$^{f/f}$; *Rosa26-mT/mG,* hereafter *Ctnna1*$^{\Delta\beta/\Delta\beta}$ and *Ctnna1*$^{\Delta\alpha/\Delta\alpha}$
388 mice, respectively). The *Rosa26-mT/mG* lineage-tracing allele faithfully reported the *Ins1-Cre* and
389 *Gcg-iCre* cell lineages at P7 (Figure 5A-5H), allowing examination of the respectively labeled β-
390 and α-cells using mGFP expression. The mGFP^{+} β-cells of *Ctnna1*$^{\Delta\beta/+}$ mice are mostly located on
391 the islet core (Figure 5A,5E), and the mGFP^{+} α-cells of *Ctnna1*$^{\Delta\alpha/+}$ mice are mostly located in the
392 islet mantle (Figure 5C,5G). Additionally, we found that β-cells exhibited strong F-actin condensed
393 cellular junctions with well-organized rosette structures (S7B, yellow arrows). In contrast, α-cells
394 displayed loosely bundled F-actin assemblies without focal-condensed junctional structures found
395 in control mice (Figure S7D, yellow arrows), supporting the notion that α-cells may have relatively
396 low adhesive properties. Inactivation of Ctnna1 in β-cells and α-cells significantly diminished the
397 formation of F-actin, as indicated in Figure S7C and S7E (highlighted by yellow arrows). This
398 suggests a substantial decrease in cell adhesion assemblies within the β-cells of *Ctnna1*$^{\Delta\beta/\Delta\beta}$ and
399 the α-cells of *Ctnna1*$^{\Delta\alpha/\alpha}$ islets.
400
401 Based on the DAH proposed by previous studies, we expected that Ctnna1-expressing α-cells
402 would tend to cluster together and become more concentrated towards the center of *Ctnna1*$^{\Delta\beta/\Delta\beta}$
403 islets due to weaker adhesion in β-cells lacking Ctnna1. Our observations supported this

404 hypothesis: in *Ctnna1*$^{\Delta\beta/\Delta\beta}$ islets, where only β-cell adhesion was affected but not α-cell adhesion,
405 we observed a significant decrease in α-cells at the periphery and an increase in their density at
406 the core of the islets (Figure 5B, 5F, 5I). Additionally, our data revealed that islet core-located α-
407 cells had a higher tendency to form clusters (Figure 5F). These results are consistent with the
408 prediction of DAH that cells with stronger adhesion tend to exclude those with weaker adhesion
409 and to form a cluster with a defined size.
410
411 However, in α-cell-specific Ctnna1-deletion (*Ctnna1*$^{\Delta\alpha/\Delta\alpha}$) mutants, we observed a reduction in α-
412 cells at the periphery and an increase in their frequency in the islet core (Figure 5D, 5H, 5J), which
413 was unexpected based on the predictions of DAH. Nevertheless, the core-located Ctnna1-
414 deficient α-cells were mostly scattered as single cells without clustering together in the islet of
415 *Ctnna1*$^{\Delta\alpha/\Delta\alpha}$ mice (Figure 5H). This suggests that the role of Ctnna1 in regulating cellular
416 distribution within the islets may be more complex than the simple attractor-repeller mechanism
417 proposed by DAH. These observations support the idea that differential adhesion between
418 endocrine subtypes is a contributing factor for establishing the islet architecture during
419 development; and the weaker cell adhesion in the peripheral islet layers leads to the specific loss
420 of these cell types in *Ctnna1*$^{\Delta Endo/\Delta Endo}$ islets.
421
422 *Coordination of ECM and cell-cell adhesion regulates islet vascularization, architecture, and*
423 *functional maturation.*
424 Our studies have shown that the coordination of cell-ECM and cell-cell adhesion plays a vital role
425 in regulating islet development. These adhesions work together to balance interactions between
426 endocrine cells and blood vessels. When one of these adhesions is perturbed, islet endocrine
427 cells may compensate with another interaction to maintain islet aggregation (Figure S5I). However,
428 it is still unclear whether islet clustering relies solely on these two adhesions. To test this, we
429 generated *Ngn3-Cre; Ctnna1*$^{f/f}$*; Itgb1*$^{f/f}$ (hereafter *Ctnna1; Itgb1*$^{\Delta Endo/\Delta Endo}$) double knockout (DKO)
430 mice, in which we simultaneously removed cell-ECM and cell-cell adhesion in all endocrine
431 progenitor cells. We compared control, *Ctnna1*$^{\Delta Endo/\Delta Endo}$*, Itgb1*$^{\Delta Endo/\Delta Endo}$ and DKO islets at P7 to
432 examine their morphology.
433
434 At P7, *Ctnna1*$^{\Delta Endo/\Delta Endo}$ islets displayed loosely aggregated endocrine cells, increased
435 vascularization (Figure 6A, 6B), reduced F-actin assemblies, and more active-Itgb1^{+} endothelial
436 cells in the loosened islet aggregates (Figure S8A, S8B). Conversely, *Itgb1*$^{\Delta Endo/\Delta Endo}$ islets
437 clumped together (Figure 6C), with strong F-actin assemblies and less active-Itgb1^{+} endothelial
438 cells in the tightly aggregated islets (Figure S8C). However, the aggregation of endocrine cells
439 was completely abrogated in the DKO mice (Figure 6D). These DKO endocrine cells became
440 suspended single cells scattered throughout the entire pancreatic epithelium, displaying rounded
441 cell morphology (Figure 6D). The DKO endocrine cells were larger and displayed weak F-actin
442 assemblies (Figure S8D). Despite the drastic changes in endocrine cell aggregation and
443 morphology, the endocrine cell subtypes were still present in the P7 DKO islets (Figure 6D and
444 data not shown), suggesting that the differentiation of endocrine subtypes is independent of the
445 islet aggregation process.
446

447 We next investigated whether the failure in islet aggregation affected endocrine cell maturation
448 by performing IF for β-cell maturation markers. In P7 control mice, Ucn3 and Glut2 were robustly
449 expressed in the cytosol and cell surface of β-cells, respectively (Figure 6E, 6I). Deletion of
450 *Ctnna1* or *Itgb1* in endocrine progenitor cells led to reduced expression of Ucn3 and Glut2 in β-
451 cells (Figure 6F, 6G, 6J, 6K), which was consistent with gene profiling analysis from 8 week old
452 mice. Finally, DKO islets displayed a severe loss of β-cell maturation markers in P7 β-cells (Figure
453 6H, 6L). In addition, while endocrine cells in normal islets do not express progenitor markers Sox9
454 or Spp1 at P7 (Figure S8E, S8G), the endocrine cells in the DKO islets exhibited elevated
455 expression of these markers at P7 (Figure S8F, S8H). These findings suggest that β-cell
456 maturation is linked to the cell adhesion-mediated islet aggregation process.
457
458 To investigate whether the islet aggregation and β-cell maturation defects in DKO mice at P7
459 were due to developmental delays, we examined islets during later adulthood stages. At 8 weeks,
460 normal endocrine cells form tightly aggregated islets (Figure 7A), but in DKO mice, endocrine
461 cells remain mostly scattered, forming smaller and loosely attached clusters (Figure 7B). These
462 smaller clusters of endocrine cells abnormally express progenitor markers Sox9 and Spp1 (Figure
463 7B; and data not shown). While the endocrine cells appear to be located closely to each other in
464 lower resolution images, Airyscan super-resolution images of F-actin IF on endocrine cells in DKO
465 islets showed that the endocrine cells are completely separated from each other without forming
466 discernible junction structures (Figure 7C, 7D, yellow arrows). Furthermore, the endocrine cells
467 also exhibit separation from the vasculatures in the DKO islets (Figure 7C, 7D, red arrows). These
468 observations indicate that both the islet aggregation and the β-cell maturation defects in DKO
469 mice persist into adulthood. Supporting this, low expression of β-cell maturation markers Ucn3
470 and Glut2 persisted in 8 week old DKO islets (Figure 7F-7H). These mice were severely glucose
471 intolerant (Figure 7I) and exhibit very low insulin secretion upon glucose stimulation (Figure 7J).
472 Together, our findings support a model in which islet morphogenesis, vasculature interaction,
473 endocrine cell aggregation, and the β-cell maturation process depend on cell-ECM and cell-cell
474 adhesion during development (Figure 7K).
475
476 **DISCUSSION**
477 Our study reveals the combinatorial roles of cell-ECM and cell-cell adhesion in regulating the
478 aggregation of endocrine cells into islets. Mechanistically, islet cell aggregation depends on
479 endocrine cell-cell adhesion, which is negatively regulated by cell-ECM adhesion through
480 vascular interaction. These two adhesion properties are reciprocally regulated: lowering cell-ECM
481 adhesion promotes endocrine cell-cell adhesion; and, conversely, lowering cell-cell adhesion
482 promotes cell-ECM adhesion. Importantly, the aggregation and functional maturation processes
483 of endocrine cells are affected by the loss of either adhesion property and are further affected by
484 the loss of both.
485
486 In this study, we aimed to elucidate the role of ECM signaling by specifically deleting the essential
487 ECM receptor Itgb1 during endocrine specification. Our findings demonstrate that while the
488 morphology and function of *Itgb1*$^{\Delta Endo/\Delta Endo}$ islets were impacted, the total islet area remained
489 unaffected, suggesting that Itgb1 deletion may not result in overt cell death in islets, unlike in other
490 organ systems (Carlson et al., 2008; Speicher et al., 2014). These observations indicate the

involvement of other mediators of cell-ECM interactions in islet maintenance. Although Itgb1 is a key player in cell-ECM interactions, compensatory mechanisms involving other integrins, such as β3, β4, β5, β 6; and α3, α 6, αV integrins, may be operative in Itgb1-deficient islets. Previous studies have highlighted the critical roles of these integrins in cell-ECM interactions and islet biology (Cirulli et al., 2000; Krishnamurthy et al., 2011; Schiesser et al., 2021; Yashpal et al., 2005). It is plausible that these integrins compensate for cell-ECM interactions, ensuring the survival and function of Itgb1-deficient islets. Further investigations are warranted to comprehensively understand the compensatory mechanisms and contributions of other integrins in Itgb1-deficient islets.

Both *Itgb1*$^{\Delta Endo/\Delta Endo}$ and *Itgb1*$^{\Delta Mature\beta/\Delta Mature\beta}$ mice demonstrate reduced vascularization, highlighting the importance of ECM signaling in vascular interactions throughout stages from embryonic endocrine cells to mature β-cells. This aligns with previous research using *MIP-Cre* to create *Itgb1*-knockout mice, which also exhibited decreased islet vascularization (Win et al., 2020). The critical role of Itgb1 signaling in organ vascularization seems universal; studies indicate that Itgb1-inactivation in pituitary endocrine epithelial cells and kidney cells leads to a loss of vasculature (Mohamed et al., 2020; Scully et al., 2016). Reduced vascular interaction can instigate hypoxia responses, which have been tied to β-cell maturation processes (Balboa et al., 2022; Heinis et al., 2010; Zeng et al., 2017). We thus propose that the impaired β-cell maturation observed in *Itgb1*$^{\Delta Endo/\Delta Endo}$ mice could stem from a hypoxic state caused by vascular loss. However, this hypothesis requires further empirical investigation for validation.

The expression of *Vegfa*, an essential growth factor for islet vasculature, is not affected in *Itgb1*$^{\Delta Endo/\Delta Endo}$ islets (Table S1). Thus, the reduced vascularization in Itgb1-deficient islets may not be explained by the lack of Vegfa. Downstream of Integrin signaling, integrin-linked kinase (ILK) is activated upon Integrin-ECM binding to regulate actin organization, cell migration, and other cellular processes (Hannigan et al., 2005). Genetic deletion of ILK in the developing pancreas leads to the failure of ILK-inactivated endocrine cells to adhere to the basement membrane, and drastic reduction of intra-islet blood vessel density (Kragl et al., 2016). This study further showed that cortical actomyosin contraction was significantly increased, thus increasing cortex tension in both the ILK-deleted islets, as well as in Itgb1-inactivated cultured β-cells. Our analyses showed aberrant organization of F-actin fibers and compaction of individual endocrine cells, as well as dysregulated cytoskeleton genes in *Itgb1*-deleted islets. Thus, it is likely that both the *Itgb1*$^{\Delta Endo/\Delta Endo}$ and *Itgb1*$^{\Delta Mature\beta/\Delta Mature\beta}$ islets fail to interact with vasculature resulting in the same alteration of the actomyosin regulation seen in ILK-deleted islet cells. In contrast, the *Ctnna1*$^{\Delta Endo/\Delta Endo}$ model shows increased islet vascularization without affecting the expression of *Vegfa* (Table S2). We posit that weakened adhesion between endocrine cells in *Ctnna1*$^{\Delta Endo/\Delta Endo}$ islets may allow greater penetration of vasculature through islet clusters, leading to augmented islet vascularization. Supporting this notion, salivary gland patterning allows vessel penetration via an epithelial "cleft" created by weakened cell-cell adhesion (Kwon et al., 2017). Interestingly, the initial steps of cleft formation requires ECM-Itgb1 signaling (Sakai et al., 2003); conversely, reducing cell-cell adhesion promotes cell-ECM adhesion during budding morphogenesis (Wang et al., 2021). Thus, our proposed model, in which ECM signaling in concert with cell-cell adhesion controls islet aggregation, may reflect a fundamental mechanism of organ morphogenesis.

535
536 In the context of our findings, it is crucial to consider the potential role of vascular alignment in
537 islet cell function. The vasculature system within the islet plays an indispensable role not only in
538 delivering nutrients to the cells but also in facilitating the efficient distribution of hormones into the
539 peripheral circulation (Gan et al., 2018). The functional maturation of β-cells and their efficiency
540 in hormone secretion are likely influenced by their proximity to and interaction with the vasculature.
541 In our *Itgb1* and *Ctnna1* deficient models, we observed an abnormal aggregation of islet cells,
542 resulting in scattered cells that appear misaligned with the vasculature. This disorganization could
543 potentially impair nutrient delivery and hormone distribution, further exacerbating the functional
544 impairments seen in these models. It is plausible that, in addition to their impact on cell-cell
545 adhesion and aggregation, the inactivation of Itgb1 and Ctnna1 may also interfere with the proper
546 integration of β-cells with the islet vasculature. This perspective adds another layer to our
547 understanding of the complex interplay between cellular adhesion, aggregation, and the
548 vasculature in islet morphology and function.
549
550 The onset of the proendocrine cell program triggers the expression of Ngn3, a factor thought to
551 stimulate the activation of ECM signaling. This signaling pathway is regarded as a key regulatory
552 mechanism controlling the delamination and migration of proendocrine cells away from ductal
553 progenitor cords (Rosenberg et al., 2010). In the case of *Itgb1*$^{\Delta Endo/\Delta Endo}$ mice, the deactivation of
554 ECM signaling in these endocrine progenitors leads to a noticeable decrease in their migration
555 distances. Consequently, differentiated endocrine cells remain entangled with ducts post-
556 differentiation from as early as E15.5, highlighting the role of ECM signaling in facilitating
557 endocrine progenitor migration during initial developmental stages. Interestingly, this
558 phenomenon of reduced migration is not observed in *Itgb1*$^{\Delta Mature\beta/\Delta Mature\beta}$ islets, suggesting the
559 impact of ECM signaling on cell migration may be more specific to the progenitor stage.
560 Supporting this hypothesis, studies utilizing *Ins-Cre* or *RIP-Cre* to ablate Itgb1 in post-
561 differentiated insulin-producing cells have reported no discernible migration defects (Diaferia et
562 al., 2013; Win et al., 2020). During the limited time window of endocrine cell development, islet
563 cell radial migration is also modulated by semaphorin signaling (Pauerstein et al., 2017). The
564 remodeling of actin, induced by semaphorin, is associated with changes in the cell's anchorage
565 to the ECM (Alto and Terman, 2017). This suggests that the chemoattractant system, where
566 semaphorin signaling occurs, could potentially intersect with the activation of Itgb1 signaling. This
567 intersection of signaling pathways may guide the migration of islet progenitor cells toward the
568 periphery and away from the ducts. Thus, the chemoattractant system where semaphorin
569 signaling occurs may involve the activation of Itgb1 signaling to control islet progenitor cell
570 migration toward the periphery, and away from the ducts. Whether the migration of endocrine
571 progenitors toward the periphery affects their function, remains to be tested. However, the role of
572 ECM-Integrin signaling extends beyond the scope of cell migration. In adult stages, ECM-Integrin
573 signaling continues to have a significant impact on differentiated endocrine cells within pancreatic
574 islets (Gan et al., 2018). Therefore, when we use the term "endocrine cells" in this study, we refer
575 to both progenitor and differentiated cells, and the significance of ECM-Integrin signaling spans
576 across multiple cellular processes, not being confined to migration alone.
577

578 Despite the endocrine subtype ratios being different in human versus rodent islets, the precise
579 differences in the stereotypical architectures in the two species have been debated. Studies using
580 different imaging modalities have yielded different conclusions (Dybala et al., 2020). In mice, it is
581 proposed that spatiotemporal collinearity leads to the typical core-mantle architecture of the
582 spherical islet in which α-cells, the first to develop, form the peninsular outer layer, and β-cells
583 subsequently form beneath them (Sharon et al., 2019a). Our current study has not directly tested
584 this hypothesis, yet our observations suggest that differential cell adhesion is critical for
585 developing this structure. Our data support a model in which randomly allocated α- and β-cells
586 are specified and sorted into the final islet architecture based on differential adhesion. It remains
587 to be tested whether the differential cell adhesion is also involved in the development of islet
588 architectures in human. In addition, studies have shown that the Roundabout (Robo)/Slit signaling
589 axis plays a role in determining islet stereotypical architecture. The secreted ligand, Slit, is often
590 associated with the ECM, and binds to Robo receptors to control various cellular responses via
591 cytoplasmic kinases and the regulation of actin and microtubule cytoskeleton (Jiang et al., 2022;
592 Tong et al., 2019). Mice lacking *Robo1* and *Robo2* in all endocrine cells, or selectively in β cells,
593 show complete loss of endocrine cell type sorting in the islets (Adams et al., 2021; Adams et al.,
594 2018; Gilbert et al., 2020). Interestingly, Robo1/2 double knockout islets exhibit adhesion defects
595 and are prone to dissociate upon isolation (Adams et al., 2018), similar to the *Ctnna1*$^{\Delta Endo/\Delta Endo}$
596 islets. Similar observations have been shown in stem cell sorting and cancer cell migration;
597 binding of Slit to Robo receptors leads to the modulation of Ncad- or Ecad-mediated cell adhesion
598 (Stine et al., 2014; Tong et al., 2019). We speculate that Robo/Slit signaling regulates endocrine
599 cell type sorting in islets by controlling cell adhesive properties to establish the islet architecture.
600
601 **Limitation of the study**
602 Our study's potential limitation is the use of the *Ngn3-Cre* driver for targeted gene deletion. While
603 commonly used for pancreatic endocrine progenitor and its lineage-specific gene deletion, *Ngn3*
604 is also expressed in other tissues such as the brain and gastrointestinal tract (Schonhoff et al.,
605 2004; Simon-Areces et al., 2010). Deletion of genes using this driver could impact these other
606 tissues and create unintended consequences. Previous studies show that *Ctnna1* deletion in
607 neuronal progenitor cells in the brain can lead to altered neural cell proliferation and differentiation
608 (Lien et al., 2006). Although we did not investigate the potential effects of *Itgb1* and *Ctnna1*
609 deletion in these other tissues, further studies are necessary to comprehend the role of ECM
610 signaling and cell adhesion in these other tissues and the potential consequences of their deletion
611 using the *Ngn3-Cre* driver.
612
613 We acknowledge the intricate interplay between cell-ECM and cell-cell interactions and
614 understand that the loss of one type of interaction does not universally enhance the other. This
615 complexity was exemplified in our double knockout model, which did not exhibit the expected
616 compensatory behaviors. While our *in vitro* model provided some insight, we recognize its
617 limitations in fully mirroring the dynamic and sophisticated changes occurring *in vivo*.
618 Consequently, our observations serve as preliminary findings that pave the way for more
619 comprehensive investigation. Further research, particularly in more complex, dynamic models,
620 will be vital in elucidating the precise nature of these interactions and their role in cell development
621 and function. The dynamic nature of islet aggregation and endocrine subtype sorting would

622 require more in-depth live imaging analysis. Obtaining 3D cellular information in developing islets
623 would provide insights into these dynamic and complex phenomena, and further our
624 understanding of the process of islet development and morphogenesis. We anticipate that using
625 pancreas slice cultures (Panzer et al., 2020) to develop an imaging platform to monitor the
626 development of live neonatal islets would provide a framework for understanding how islets
627 develop, and offer novel ways to harness this understanding in the search for clinical alternatives
628 to treat diabetes.

AUTHOR CONTRIBUTIONS

W.T., M.M., Y.T.C., W.Y. and H.P.S. conceived the project, designed the experiments, and analyzed the data. W.T., M.M., Y.T.C. performed the analysis of mouse genetic models and live-imaging experiments. Y.T.C performed *in vitro* islet cell aggregation assay. A.C. assembled figures and graphical summaries. N.P. and S.D. analyzed the RNA-seq data and generated heatmaps. M.N. performed segmentation analysis. P.F. performed hyperglycemic clamp experiment. R.H and M.H. analyzed *Ucn3-Cre* mouse model and prepared gene expression genome viewer plots. S.W., W.J.H., and J.L.K. conceived *Ctnna1-flox* mouse breeding and experiments. W.T., M.M., and H.P.S. wrote the manuscript.

ACKNOWLEDGEMENTS

We acknowledge the support of City of Hope Core Facilities: Dr. Brain Armstrong from the Microscopy Core, Dr. Zhuo Li from the Electron Microscopy Core, Drs. Xiwei Wu and Min-Hsuan Chen from the Integrative Genomics Core, Dr. Patrick Fueger from the Comprehensive Metabolic Phenotyping Core at City of Hope. We thank Dr. Maike Sander for sharing the anti-Ngn3 antiserum and Dr. Rupangi Vasavada for sharing the *Ins-Cre* mouse strain. The California Institute for Regenerative Medicine (CIRM) Training Grant EDUC4-12772 to W.T.; JDRF postdoctoral fellowship 3-PDF-2019-742-A-N to M.M.; NSERC Discovery Grant (RGPIN-2016-04276), CIHR New Investigator Award Msh-147794, and MSFHR Scholar Award 18309 to J.L.K., NIH/NIDDK 1R01DK110276 to M.O.H.; NIH/NIDDK 1R01DK120523, Human Islet Research Network (HIRN) New investigator Award (subaward via UC4DK104162), and a grant from the Wanek Family Foundation to Cure Type 1 Diabetes to S.D.; Wanek Family Foundation to Cure Type 1 Diabetes and NIH/NIDDK 1R01DK119590 to H.P.S.. We acknowledge the assistance of OpenAI's ChatGPT in refining the language and grammar of our manuscript during resubmission. The contributions of this AI model were strictly limited to textual improvements, with no role in generating or modifying the scientific content and findings of the study.

656 **FIGURES**

FIGURE 1

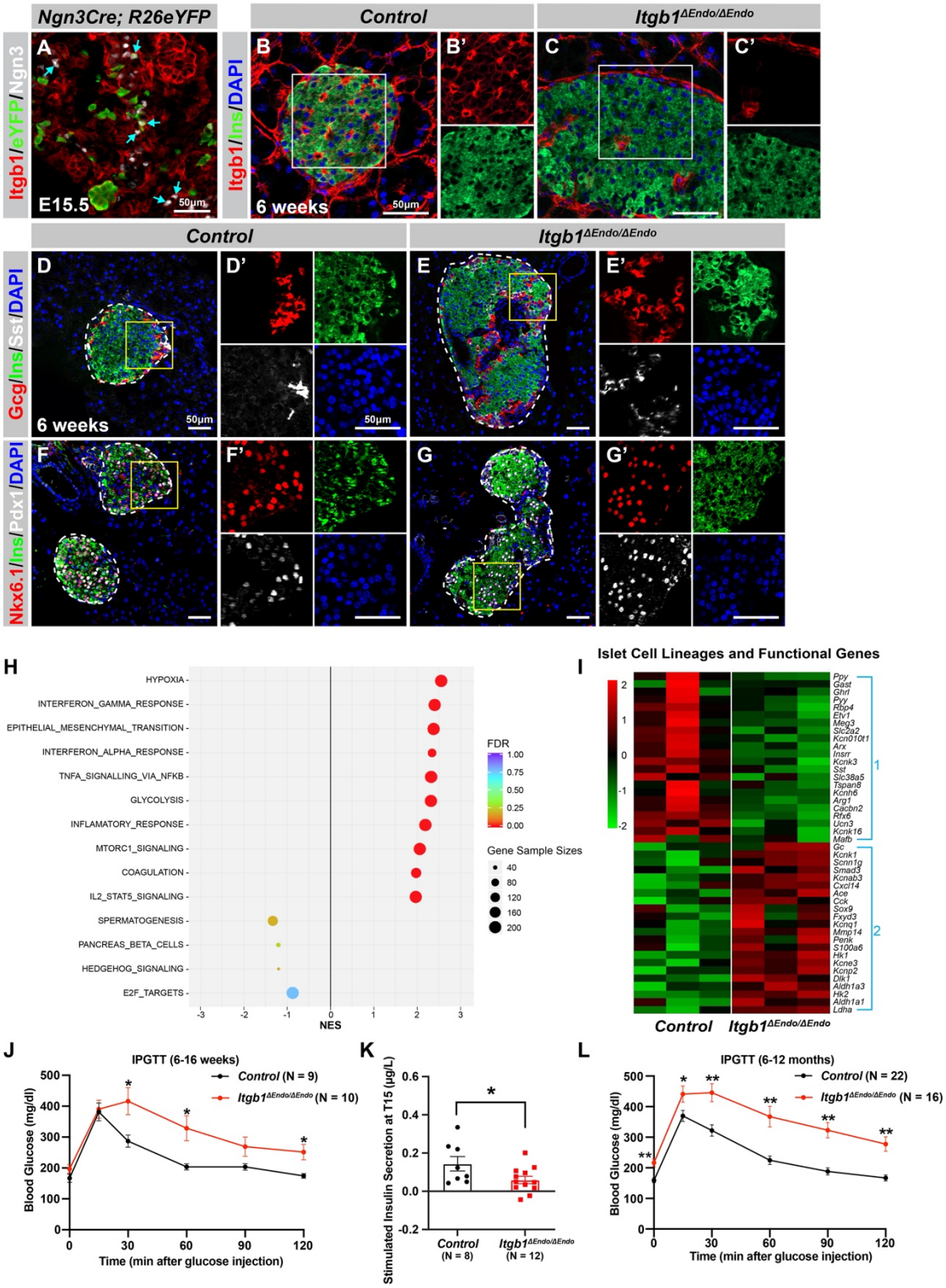

657

658 **Figure 1. ECM-Itgb1 signaling in endocrine progenitors is required for normal islet**
659 **morphology and function.**
660 A) Immunofluorescence staining for Itgb1 and Ngn3 in pancreas sections of *Ngn3-Cre;*
661 *Rosa26eYFP* reporter mice at E15.5. Cyan arrows indicate Ngn3^{+} cells and lineage-traced
662 endocrine cells expressing Itgb1.
663 (B-C) Immunofluorescence staining for Itgb1, Ins, and DAPI on pancreas sections, demonstrating
664 significant *Itgb1* deletion in an *Itgb1*$^{\Delta Endo/\Delta Endo}$ islet at 6 weeks old. Fields demarcated by white
665 boxes in B-C are shown with individual color channels in B'-C' side panels.
666 (D-G) Immunofluorescence staining for Gcg, Ins, Sst, Nkx6.1, Pdx1, and DAPI on pancreas
667 sections of (D,F) control and (E,G) *Itgb1*$^{\Delta Endo/\Delta Endo}$ mice at 6 weeks old. Individual islets are
668 outlined by dotted lines. Fields demarcated by yellow boxes in D-G are shown at higher
669 magnification in D'-G' side panels.
670 (H) Gene-set enrichment analysis of the differentially expressed genes, indicating top enriched
671 pathways for control versus *Itgb1*$^{\Delta Endo/\Delta Endo}$ islets at 6 weeks old. Gene sample sizes and FDRs
672 are indicated by the size and color of the dots.
673 (I) Heatmap demonstrating down-regulation (Group 1) and up-regulation (Group 2) of functional
674 maturation genes in *Itgb1*$^{\Delta Endo/\Delta Endo}$ islets compared to controls.
675 (J-L) Intraperitoneal glucose tolerance test (J,L) and stimulated insulin secretion at T15 (K) on 6
676 to 16 weeks old (J,K) and (L) 6 to 12 months old control and *Itgb1*$^{\Delta Endo/\Delta Endo}$ mice.
677
678 Ngn3, Neurogenin 3; Gcg, Glucagon; Ins, Insulin; DAPI, 4',6-diamidino-2-phenylindole; Sst,
679 Somatostatin; IPGTT, intraperitoneal glucose tolerance test; FDR, false discovery rate; E15.5,
680 embryonic day 15.5
681 Data are shown as mean ± SEM. * $p < 0.05$ and ** $p < 0.01$.

SUPPLEMENTARY FIGURE 1: RELATED TO FIGURE 1

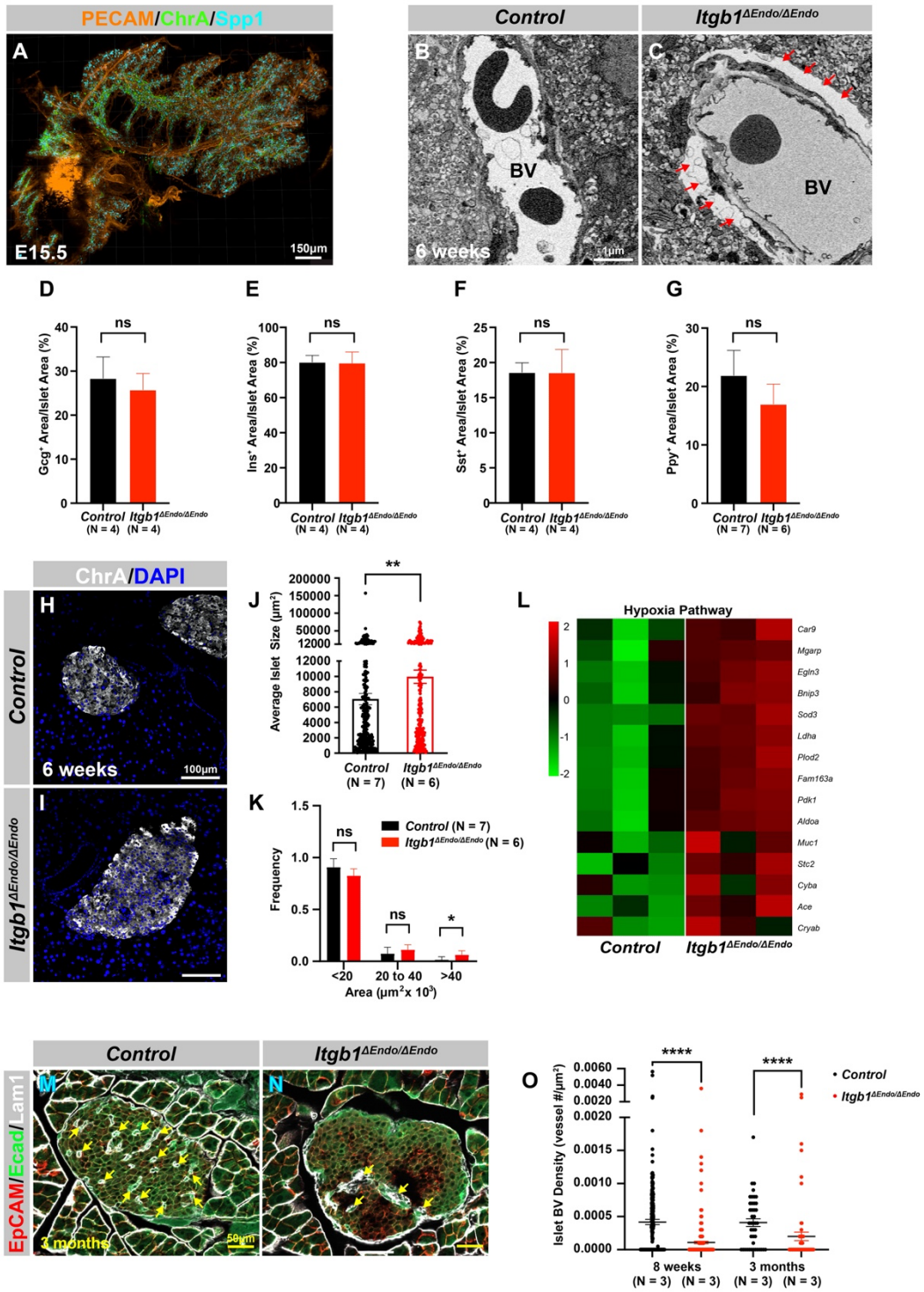

682

683 **Figure S1. Deletion of *Itgb1* in endocrine progenitors results in abnormal interactions with**
684 **blood vessels and decreased expression of functional maturation markers within islets.**
685 **Related to Figure 1.**
686 (A) Whole mount immunofluorescence staining for PECAM, ChrA, and Spp1 in a wild-type
687 pancreas at E15.5.
688 (B-C) Transmission electron microscope images showing blood vessels in 6 weeks old islets.
689 Deletion of *Itgb1* disrupts the attachment of endocrine cells to blood vessels (red arrows) in
690 *Itgb1*$^{\Delta Endo/\Delta Endo}$ islets.
691 (D-G) Quantification of the percentage of (D) Gcg^{+}, (E) Ins^{+}, (F) Sst^{+}, and (G) Ppy^{+} cells relative
692 to measured islet area of 6 weeks old control and *Itgb1*$^{\Delta Endo/\Delta Endo}$ pancreas sections.
693 (H-I) Immunofluorescence staining for ChrA, and DAPI in 6 weeks old (H) control and (I)
694 *Itgb1*$^{\Delta Endo/\Delta Endo}$ pancreas sections.
695 (J-K) Quantification of (J) average islet size and (K) islet size distribution based on ChrA staining
696 of 6 weeks old control and *Itgb1*$^{\Delta Endo/\Delta Endo}$ pancreas sections.
697 (L) Heatmap showing hypoxia pathway genes are up-regulated in *Itgb1*$^{\Delta Endo/\Delta Endo}$ islets.
698 (M-N) Immunofluorescence staining for EpCAM, Ecad, and Lam1 on 3 months old pancreas
699 sections showing reduced islet vasculature indicated by Lam1^{+} cells (yellow arrows).
700 (O) Quantification of islet blood vessel density in control or *Itgb1*$^{\Delta Endo/\Delta Endo}$ islet area at 8 weeks
701 and 3 months old.
702
703 PECAM, Platelet endothelial cell adhesion molecule-1; ChrA, Chromogranin A; Spp1, Secreted
704 Phosphoprotein 1; Gcg, Glucagon; Ins, Insulin; Sst, Somatostatin; Ppy, Pancreatic Polypeptide;
705 Ecad, E-cadherin; Epithelial cellular adhesion molecule, EpCAM; Lam1, Laminin1; BV, blood
706 vessels; E15.5, embryonic day 15.5.
707 Data are shown as mean ± SEM. * $p < 0.05$, ** $p < 0.01$, **** $p < 0.0001$.

SUPPLEMENTARY FIGURE 2: RELATED TO FIGURE 1

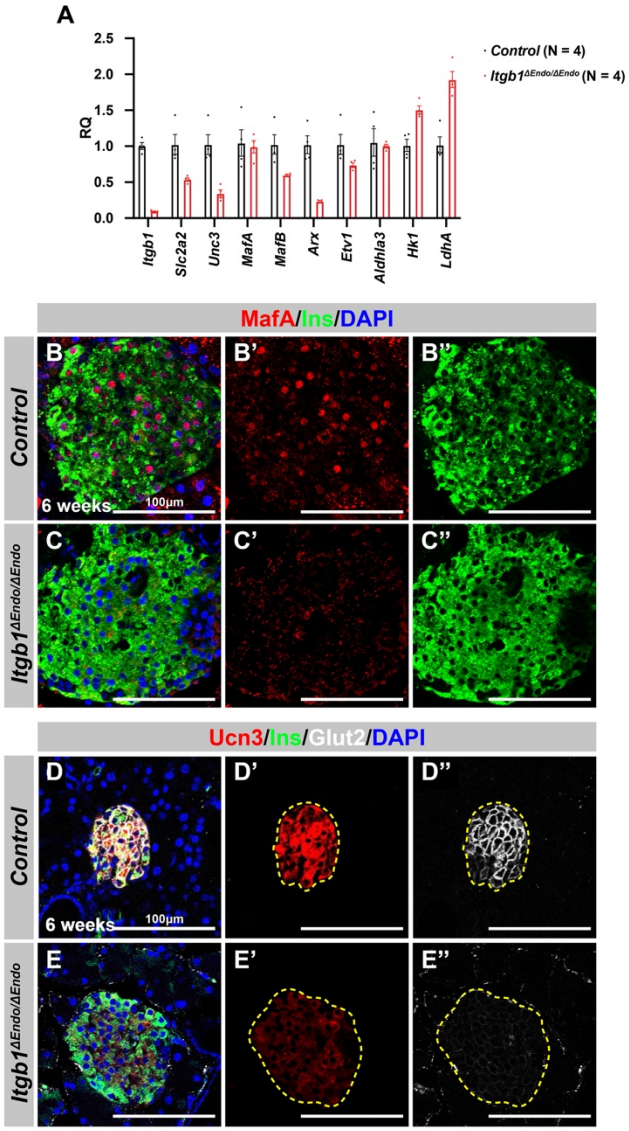

708

Figure S2. Deletion of *Itgb1* in endocrine progenitors results in abnormal interactions with blood vessels and decreased expression of functional maturation markers within islets. Related to Figure 1.

(A) Quantification of selected differentially expressed genes involved in islet functional maturation using real-time qPCR analysis in *Itgb1*$^{\Delta Endo/\Delta Endo}$ islets and compared to controls. The relative quantification of gene expression levels was determined using the $2^{-\Delta\Delta Ct}$ method and is reported as a RQ value relative to the control group. The genes selected for validation were chosen based on their known roles in islet function and maturation.

(B-E) Immunofluorescence staining for MafA, Ins, Ucn3, Glut2 and DAPI on 6 weeks old (B,D) control and (C,E) *Itgb1*$^{\Delta Endo/\Delta Endo}$ pancreas sections. Individual islets are outlined by dotted yellow lines in (D',D",E',E").

RQ, Relative quantification; Ins, Insulin; Ucn3, Urocortin 3; PECAM, Platelet endothelial cell adhesion molecule-1; DAPI, 4',6-diamidino-2-phenylindole; E15.5, embryonic day 15.5.

Data are shown as mean ± SEM. * $p < 0.05$.

FIGURE 2

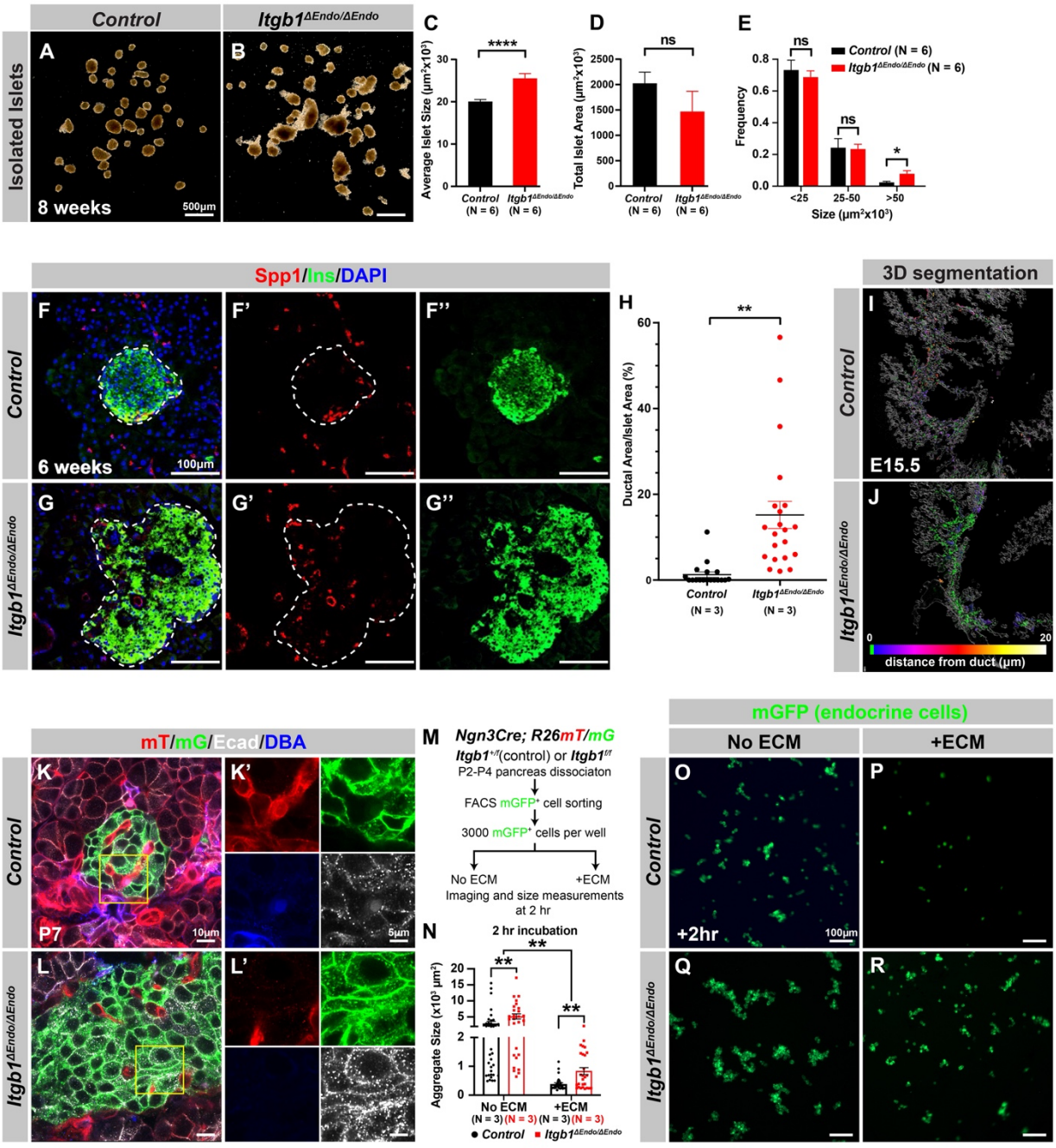
Control
Itgb1ΔEndo/ΔEndo
Isolated Islets
A
B
8 weeks
500µm
C
Average Islet Size (µm²x10³)
****
Control (N = 6)
Itgb1ΔEndo/ΔEndo (N = 6)
D
Total Islet Area (µm²x10³)
ns
E
Frequency
Control (N = 6)
Itgb1ΔEndo/ΔEndo (N = 6)
<25
25-50
>50
Size (µm²x10³)
Spp1/Ins/DAPI
F
F'
F''
G
G'
G''
6 weeks
100µm
H
Ductal Area/Islet Area (%)
**
Control (N = 3)
Itgb1ΔEndo/ΔEndo (N = 3)
3D segmentation
I
E15.5
J
distance from duct (µm)
mT/mG/Ecad/DBA
K
K'
L
L'
P7
10µm
5µm
M
Ngn3Cre; R26mT/mG
Itgb1+/f(control) or Itgb1f/f
P2-P4 pancreas dissociaton
FACS mGFP+ cell sorting
3000 mGFP+ cells per well
No ECM
+ECM
Imaging and size measurements at 2 hr
N
2 hr incubation
Aggregate Size (x10³ µm²)
No ECM
+ECM
Control
Itgb1ΔEndo/ΔEndo
mGFP (endocrine cells)
No ECM
+ECM
O
P
Q
R
+2hr
100µm

724

725
726 **Figure 2. Itgb1 signaling is required for proper endocrine progenitor aggregation.**
727 (A-B) Brightfield images of isolated islets from control and *Itgb1*$^{\Delta Endo/\Delta Endo}$ mice at 8 weeks old.
728 (C-E) Quantification of (C) average islet size, (D) total islet area, and (E) islet size distribution
729 based on morphometric analysis of 8 weeks old control and *Itgb1*$^{\Delta Endo/\Delta Endo}$ isolated islets.
730 (F-G) Immunofluorescence staining for Spp1, Ins, and DAPI on 6 weeks old control and
731 *Itgb1*$^{\Delta Endo/\Delta Endo}$ pancreas sections. Islets are outlined by white dotted lines.
732 (H) The ratio of ductal cell areas within the islets is quantified based on Spp1 and ChrA staining
733 of pancreas sections from 6-week-old control and *Itgb1*$^{\Delta Endo/\Delta Endo}$ mice. (I-J) 3D segmentation
734 analysis on whole mount immunofluorescence images of E15.5 control and *Itgb1*$^{\Delta Endo/\Delta Endo}$
735 pancreata stained for ChrA and Spp1 (white colored) reveals that the endocrine cells in the
736 *Itgb1*$^{\Delta Endo/\Delta Endo}$ pancreas are mostly retained within ducts, and the distance between endocrine
737 cells and ducts is represented by a color scale. (K-L) Airyscan super-resolution images depict
738 immunofluorescence staining for Ecad and ductal marker DBA in P7 mT/mG reporter mice
739 showing up-regulation of Ecad in the *Itgb1*$^{\Delta Endo/\Delta Endo}$ pancreas. The dot-like Ecad expression
740 pattern in super-resolution imaging represents adherens junction structures. The yellow boxes in
741 K-L demarcate fields shown at higher magnification in K'-L' side panels. (M) The schematic
742 depicts the experimental design for the *in vitro* aggregation assay. (N) Aggregate size is quantified
743 after a 2-hour incubation with or without ECM. (O-R) Fluorescence images of mGFP+ endocrine
744 progenitor aggregates after 2 hours of culture show that mGFP+ control endocrine progenitors
745 clustered (O) without ECM but remained single cells (P) with ECM. Alternatively, *Itgb1*$^{\Delta Endo/\Delta Endo}$
746 endocrine progenitors clustered (Q) without ECM or (R) with ECM.
747
748 Spp1, Secreted Phosphoprotein 1; Ins, Insulin; DAPI, 4',6-diamidino-2-phenylindole; Ecad, E-
749 cadherin; DBA, Dolichos Biflorus Agglutinin; P7, postnatal day 7; E15.5, embryonic day 15.5
750 Data are shown as mean ± SEM. * $p < 0.05$, ** $p < 0.01$ and **** $p < 0.0001$.
751

SUPPLEMENTARY FIGURE 3: RELATED TO FIGURE 2

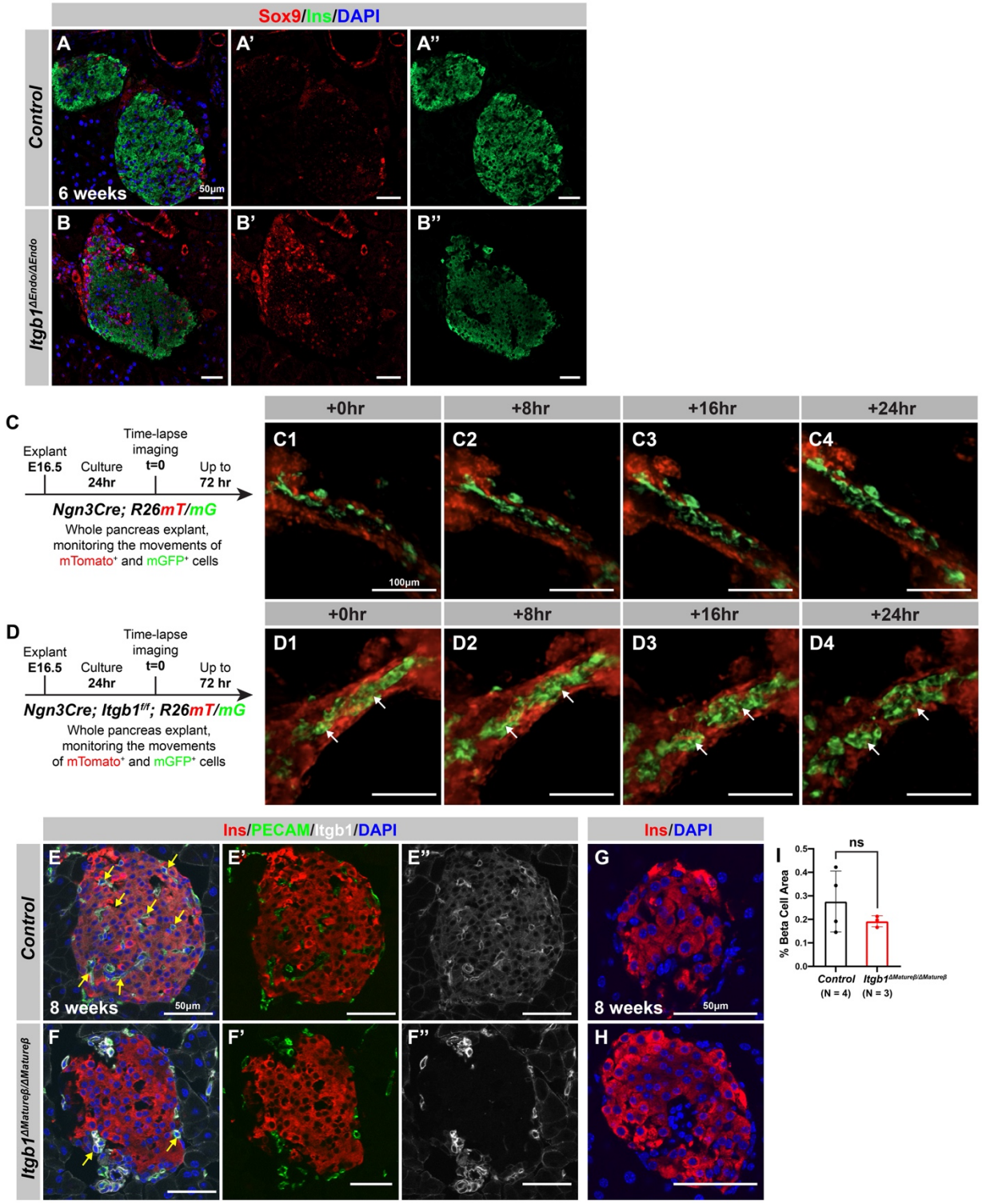

752

753 **Figure S3. Itgb1 is required for normal islet architecture. Related to Figure 2.**
754 (A-B) Immunofluorescence staining for Sox9, Ins, and DAPI on 6 weeks old (A) control and (B)
755 *Itgb1*$^{\Delta Endo/\Delta Endo}$ pancreas sections. The individual channels for Sox9 and Ins are displayed in
756 panels A' and A", and B' and B", respectively. In the *Itgb1*$^{\Delta Endo/\Delta Endo}$ islets, Sox9-positive ductal
757 cells were observed throughout the sections (B').
758 (C-D) Schematic of the time-lapse confocal microscope imaging of endocrine progenitor cell
759 behaviors in E16.5 embryonic pancreas explants. The first 24 hours were monitored to observe
760 cell movement in (C1-C4) control and (D1-D4) *Itgb1*$^{\Delta Endo/\Delta Endo}$ pancreas explants. White arrows
761 indicate prematurely clustered islets in *Itgb1*$^{\Delta Endo/\Delta Endo}$ explants.
762 (E-H) Immunofluorescence staining for Ins, PECAM, Itgb1, and DAPI on 8 weeks old (E,G) control
763 and (F,H) *Itgb1*$^{\Delta Mature\beta/\Delta Mature\beta}$ pancreas sections. Individual channels are displayed as Ins/PECAM
764 in E',F' and Itgb1 in E",F". In *Itgb1*$^{\Delta Mature\beta/\Delta Mature\beta}$ islets the presence of Itgb1 and vasculature in the
765 islet is abolished. The overall size and insulin expression are not altered in the *Itgb1*$^{\Delta Mature\beta/\Delta Mature\beta}$
766 islets.
767 (I) Quantification of total islet area based on morphometric analysis of 8 weeks old control and
768 *Itgb1*$^{\Delta Mature\beta/\Delta Mature\beta}$ pancreas sections. Note no significant differences in islet size were observed
769 between the two groups.
770
771 Ins, Insulin; PECAM, Platelet endothelial cell adhesion molecule-1; DAPI, 4',6-diamidino-2-
772 phenylindole; E16.5, embryonic day 16.5
773 Data are shown as mean ± SEM.

SUPPLEMENTARY FIGURE 4: RELATED TO FIGURE 2

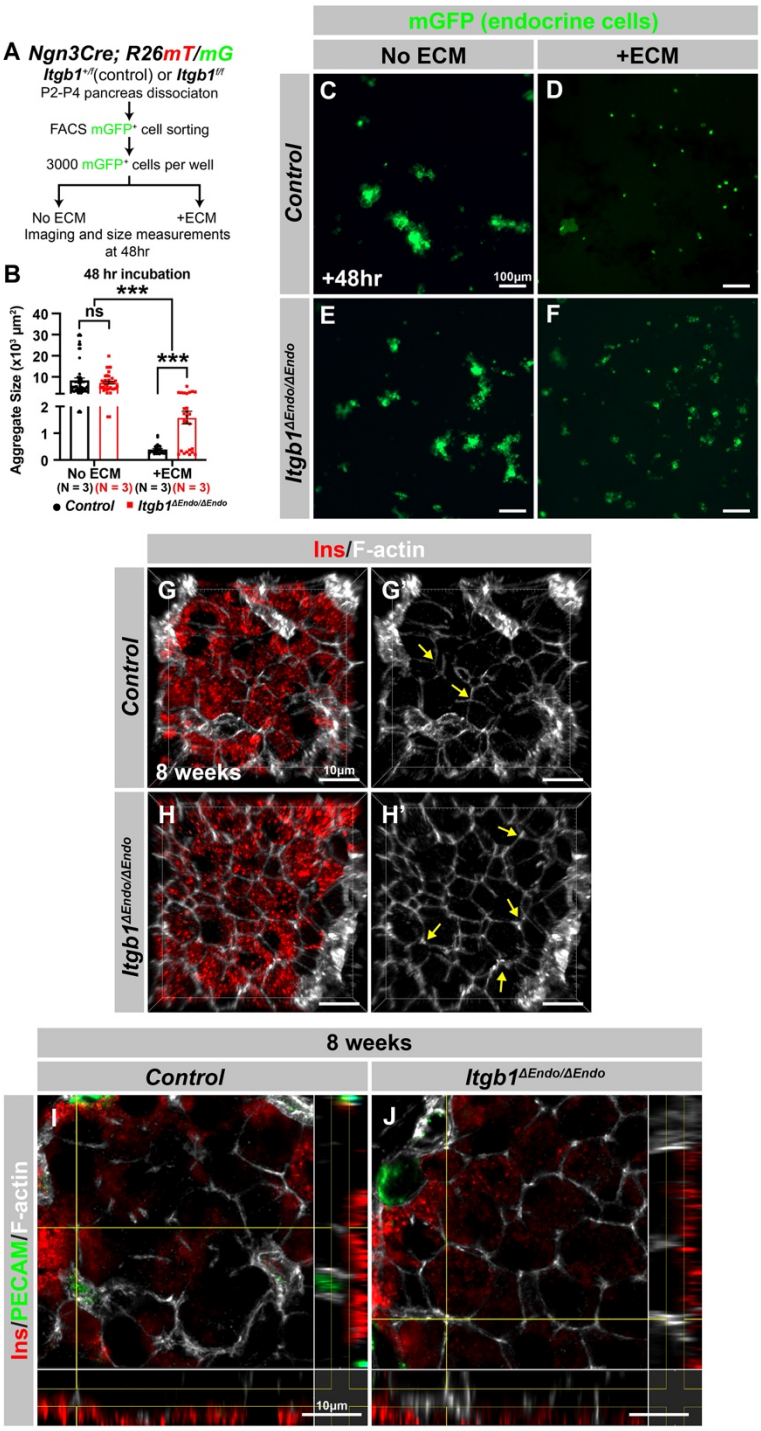

774

775 **Figure S4. Itgb1 controls cytoskeleton regulation and organization in islets. Related to**
776 **Figure 2**
777 (A) Schematic of experimental design for *in vitro* aggregation assay.
778 (B) Quantification of aggregate size after 48 hours incubation with or without ECM in control and
779 *Itgb1*$^{\Delta Endo/\Delta Endo}$ endocrine progenitors.
780 (C-F) Fluorescence images of mGFP^{+} endocrine progenitor aggregates after 48 hours
781 culture. mGFP^{+} control endocrine progenitors clustered (C) without ECM but remained single cells
782 (D) with ECM after 48 hours. Alternatively, *Itgb1*$^{\Delta Endo/\Delta Endo}$ endocrine progenitors clustered (E)
783 without ECM or (F) with ECM after 48 hours.
784 (G-J) Airyscan super-resolution 3D projection and cut-view images depict immunofluorescence
785 staining for Ins and F-actin on 8 weeks old control and *Itgb1*$^{\Delta Endo/\Delta Endo}$ pancreas sections. The 3D
786 images (G-H) and cut-view images (I-J) also demonstrated hexagonal cell shapes and increased
787 F-actin assembly in the *Itgb1*$^{\Delta Endo/\Delta Endo}$ islets.
788
789 Ins, Insulin; PECAM, Platelet endothelial cell adhesion molecule-1
790 Data are shown as mean ± SEM. *** $p < 0.001$.

FIGURE 3

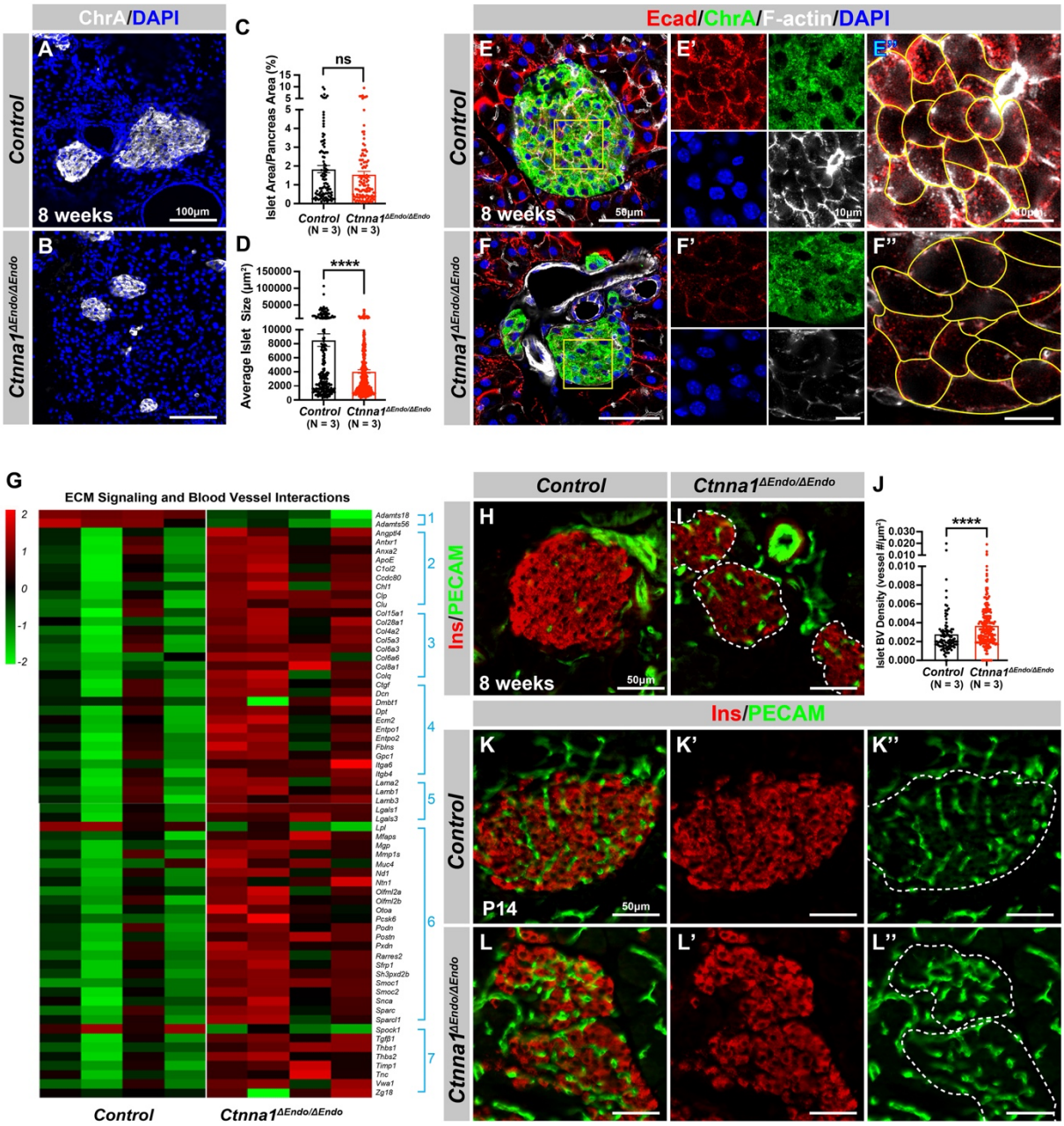
ChrA/DAPI
Control
Ctnna1ΔEndo/ΔEndo
A
B
8 weeks
100µm
C
ns
Islet Area/Pancreas Area (%)
Control (N = 3)
Ctnna1ΔEndo/ΔEndo (N = 3)
D
****
Average Islet Size (µm²)
Ecad/ChrA/F-actin/DAPI
E
E'
E''
F
F'
F''
50µm
10µm
G
ECM Signaling and Blood Vessel Interactions
Control
Ctnna1ΔEndo/ΔEndo
Ins/PECAM
H
I
8 weeks
J
Islet BV Density (vessel #/µm²)
K
K'
K''
P14
L
L'
L''

Figure 3. Ctnna1-mediated cell-cell adhesion is required for normal islet morphology and endocrine cell aggregation.

(A-B) Immunofluorescence staining for ChrA and DAPI in 8 weeks old pancreas sections showing smaller islet sizes in *Ctnna1*$^{\Delta Endo/\Delta Endo}$ mice.

(C-D) Quantification of (C) the percentage of islet area in pancreas area and (D) average islet size based on ChrA staining on 8 weeks old control and *Ctnna1*$^{\Delta Endo/\Delta Endo}$ pancreas sections.

(E-F) Airyscan images of immunofluorescence staining for Ecad, ChrA, F-actin, and DAPI for control and *Ctnna1*$^{\Delta Endo/\Delta Endo}$ pancreas sections. Fields demarcated by yellow boxes are shown at higher magnification with individual color channels in E'-F' middle panels, showing reduced expression of Ecad and F-actin in *Ctnna1*$^{\Delta Endo/\Delta Endo}$ islets. Individual endocrine cell shape is delineated by yellow lines in E"-F", demonstrating the enlarged endocrine cell sizes in the islets of *Ctnna1*$^{\Delta Endo/\Delta Endo}$ mice.

(G) Heatmap showing genes for ECM signaling and blood vessel interactions are up-regulated in *Ctnna1*$^{\Delta Endo/\Delta Endo}$ islets at 8 weeks old. Groups 1-7 represent gene ontologies of: 1) Metalloproteases, 2) Vascular Adhesion 3) Collagens, 4) Integrins, 5) Laminins, 6) Glycoproteins and 7) Thrombospondins.

(H-I) Immunofluorescence staining of Ins and PECAM on 8 weeks old control and *Ctnna1*$^{\Delta Endo/\Delta Endo}$ pancreas sections.

(J) Quantification of islet blood vessel density based on Ins and PECAM staining on 8 weeks old control and *Ctnna1*$^{\Delta Endo/\Delta Endo}$ pancreas sections.

(K-L) Immunofluorescence staining of Ins and PECAM on P14 control and *Ctnna1*$^{\Delta Endo/\Delta Endo}$ pancreas sections showing increased vasculature in *Ctnna1*$^{\Delta Endo/\Delta Endo}$ islets. Islet area is outlined by dotted lines.

ChrA, Chromogranin A; DAPI, 4',6-diamidino-2-phenylindole; Ecad, E-cadherin; Ins, Insulin; PECAM, Platelet endothelial cell adhesion molecule-1; P14, postnatal day 14

Data are shown as mean ± SEM. **** $p < 0.0001$.

SUPPLEMENTARY FIGURE 5: RELATED TO FIGURE 3

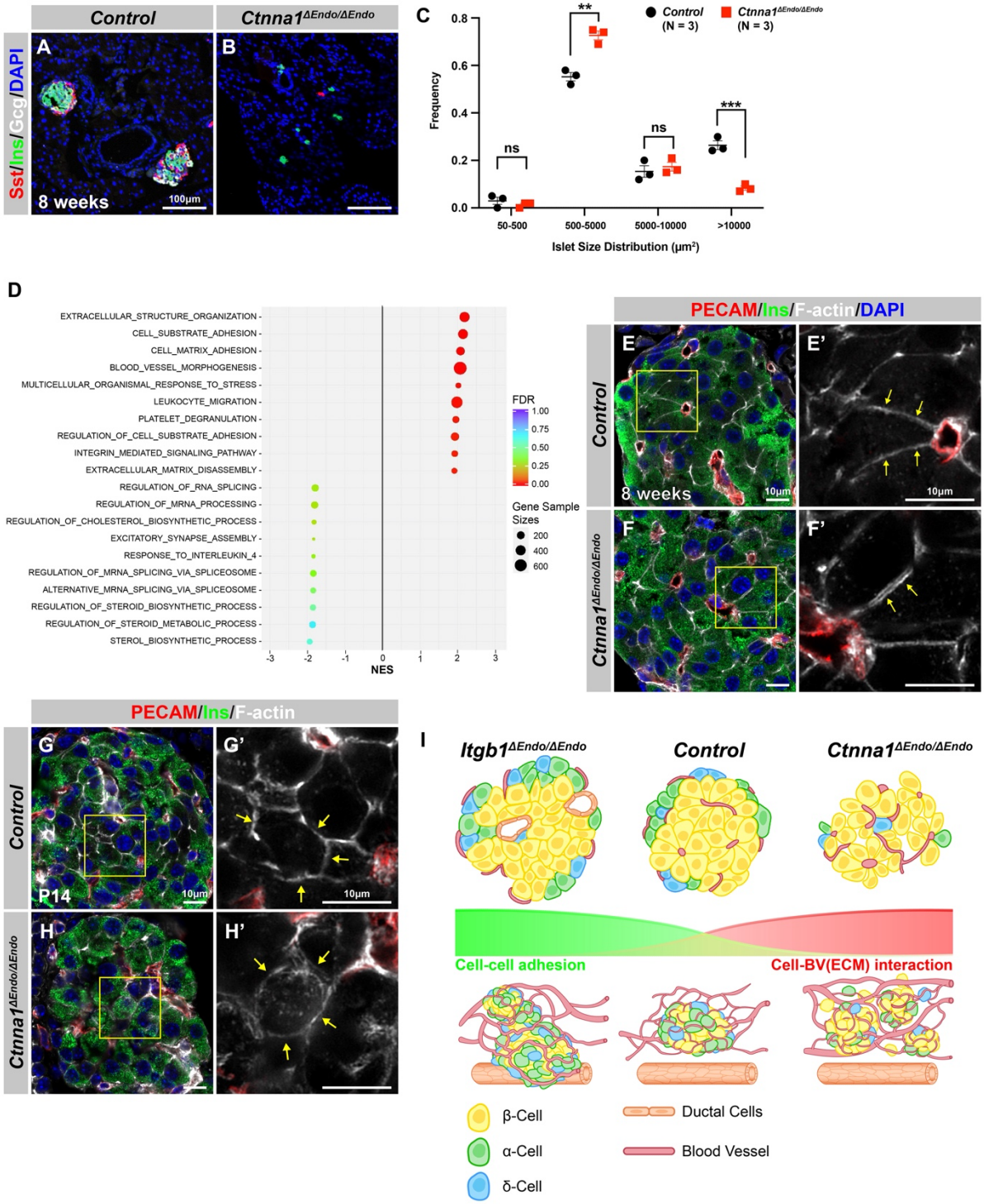

819

820 **Figure S5. *Ctnna1*-deleted pancreatic islet endocrine cells display cytoskeleton anomalies.**
821 **Related to Figure 3.**
822 (A-B) Immunofluorescence staining for Sst, Ins, and DAPI on pancreas sections from 8 weeks old
823 mice. In *Ctnna1*$^{\Delta Endo/\Delta Endo}$ mice, the islet clusters appear much smaller compared to the control
824 mice.
825 (C) Quantification of islet size distribution based on ChrA staining for 8 weeks old control and
826 *Ctnna1*$^{\Delta Endo/\Delta Endo}$ pancreas sections. The islet size quantification analysis excluded endocrine cell
827 clusters with fewer than five cells.
828 (D) Gene-set enrichment analysis of the differentially expressed genes, indicating top enriched
829 pathways for control versus *Ctnna1*$^{\Delta Endo/\Delta Endo}$ islets at 8 weeks old. Gene sample sizes and FDRs
830 are indicated by the size and color of the dots.
831 (E-F) 3D Airyscan images of immunofluorescence staining for PECAM, Ins, and F-actin on 8
832 weeks old control and *Ctnna1*$^{\Delta Endo/\Delta Endo}$ pancreas sections. Fields demarcated by yellow boxes in
833 E,F are shown at higher magnification in E',F'. The images showed the separation of F-actin
834 between Ins-expressing endocrine cells. This separation is highlighted by the yellow arrows in F'.
835 (G-H) Airyscan images of immunofluorescence staining for PECAM, Ins, and F-actin in P14
836 control and *Ctnna1*$^{\Delta Endo/\Delta Endo}$ pancreas sections. In control islets (G'), the F-actin assemblies
837 appear condensed, as indicated by the yellow arrows. However, in *Ctnna1*$^{\Delta Endo/\Delta Endo}$ islets (H'),
838 the same F-actin assemblies appear to be diffused within the insulin-expressing cells. (I)
839 Graphical summary showing cell-cell adhesion and cell-blood vessel (BV) interaction differences
840 observed in *Itgb1*$^{\Delta Endo/\Delta Endo}$ and *Ctnna1*$^{\Delta Endo/\Delta Endo}$ islets.
841
842 PECAM, Platelet endothelial cell adhesion molecule-1; Ins, Insulin; P14, postnatal day 14; BV,
843 blood vessels
844 Data are shown as mean ± SEM. ** $p < 0.01$ and *** $p < 0.001$.

FIGURE 4

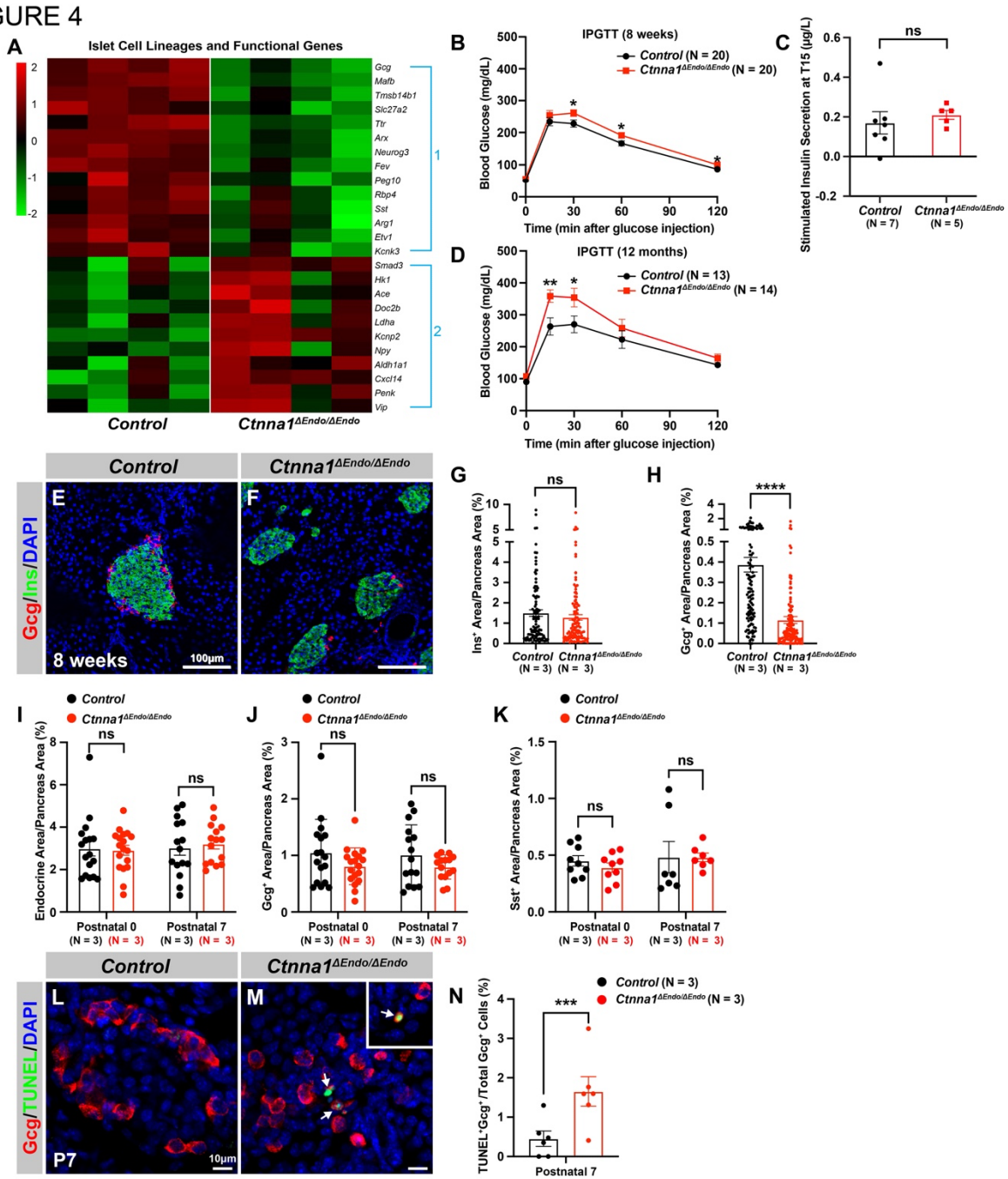
A
Islet Cell Lineages and Functional Genes
Gcg
Mafb
Tmsb14b1
Slc27a2
Ttr
Arx
Neurog3
Fev
Peg10
Rbp4
Sst
Arg1
Etv1
Kcnk3
Smad3
Hk1
Ace
Doc2b
Ldha
Kcnp2
Npy
Aldh1a1
Cxcl14
Penk
Vip
Control
Ctnna1ΔEndo/ΔEndo
B
IPGTT (8 weeks)
Control (N = 20)
Ctnna1ΔEndo/ΔEndo (N = 20)
Blood Glucose (mg/dL)
Time (min after glucose injection)
C
ns
Stimulated Insulin Secretion at T15 (µg/L)
Control (N = 7)
Ctnna1ΔEndo/ΔEndo (N = 5)
D
IPGTT (12 months)
Control (N = 13)
Ctnna1ΔEndo/ΔEndo (N = 14)
Blood Glucose (mg/dL)
Time (min after glucose injection)
Control
Ctnna1ΔEndo/ΔEndo
Gcg/Ins/DAPI
E
F
8 weeks
100µm
G
ns
Ins+ Area/Pancreas Area (%)
Control (N = 3)
Ctnna1ΔEndo/ΔEndo (N = 3)
H
****
Gcg+ Area/Pancreas Area (%)
Control (N = 3)
Ctnna1ΔEndo/ΔEndo (N = 3)
I
Control
Ctnna1ΔEndo/ΔEndo
ns
Endocrine Area/Pancreas Area (%)
Postnatal 0 (N = 3) (N = 3)
Postnatal 7 (N = 3) (N = 3)
J
Control
Ctnna1ΔEndo/ΔEndo
ns
Gcg+ Area/Pancreas Area (%)
Postnatal 0 (N = 3) (N = 3)
Postnatal 7 (N = 3) (N = 3)
K
Control
Ctnna1ΔEndo/ΔEndo
ns
Sst+ Area/Pancreas Area (%)
Postnatal 0 (N = 3) (N = 3)
Postnatal 7 (N = 3) (N = 3)
Control
Ctnna1ΔEndo/ΔEndo
Gcg/TUNEL/DAPI
L
M
P7
10µm
N
Control (N = 3)
Ctnna1ΔEndo/ΔEndo (N = 3)
***
TUNEL+Gcg+/Total Gcg+ Cells (%)
Postnatal 7

845

846 **Figure 4. Ctnna1 is required for proper islet functionality and α-cell survival.**
847 (A) Heatmap showing the top up-regulated (Group 1) and down-regulated (Group 2) endocrine
848 cell lineage and functional genes in *Ctnna1*$^{\Delta Endo/\Delta Endo}$ islets from 8 weeks old mice.
849 (B-D) The figure shows the results of the intraperitoneal glucose tolerance test (B,D) and
850 stimulated insulin secretion assay (C) performed on control and *Ctnna1*$^{\Delta Endo/\Delta Endo}$ mice at 8 weeks
851 old (B,C) and 12 months old (D). The *Ctnna1*$^{\Delta Endo/\Delta Endo}$ mice exhibited glucose intolerance, but no
852 detectable difference in insulin secretion compared to control littermates. The *Ctnna1*$^{\Delta Endo/\Delta Endo}$
853 mice are glucose intolerant with non-detectable insulin secretion defects.
854 (E-F) Immunofluorescence staining for Gcg, Ins, and DAPI on 8 weeks old (E) control and (F)
855 *Ctnna1*$^{\Delta Endo/\Delta Endo}$ pancreas sections showing a reduction of α-cells.
856 (G-H) Quantification of (G) Ins$^+$ and (H) Gcg$^+$ area relative to total pancreas area in 8 weeks old
857 control and *Ctnna1*$^{\Delta Endo/\Delta Endo}$ pancreas sections.
858 (I-K) Quantification of endocrine cell area (I), Gcg$^+$ (J), and Sst$^+$ (K) relative to total pancreas area
859 in control and *Ctnna1*$^{\Delta Endo/\Delta Endo}$ pancreas sections at P0 and P7. Note that there was no significant
860 difference observed between the control and *Ctnna1*$^{\Delta Endo/\Delta Endo}$ pancreas sections at P0 and P7.
861 (L-N) Immunofluorescence staining for Gcg, TUNEL, and DAPI on P7 control and
862 *Ctnna1*$^{\Delta Endo/\Delta Endo}$ pancreas sections. White arrows indicate TUNEL$^+$/Gcg$^+$ cells. The percentage
863 of TUNEL$^+$/Gcg$^+$ co-positive cells relative to total Gcg$^+$ cell numbers in P7 control and
864 *Ctnna1*$^{\Delta Endo/\Delta Endo}$ islets is shown in panel (N), and compared to controls, the *Ctnna1*$^{\Delta Endo/\Delta Endo}$ islets
865 exhibited significantly more TUNEL$^+$/Gcg$^+$ cells at P7.
866
867 Gcg, Glucagon; Ins, Insulin; DAPI, 4',6-diamidino-2-phenylindole; IPGTT, intraperitoneal glucose
868 tolerance test; TUNEL, terminal deoxynucleotidyl transferase dUTP nick end labeling; P0,
869 postnatal day 0; P7, postnatal day 7
870 Data are shown as mean ± SEM. * $p < 0.05$, ** $p < 0.01$, *** $p < 0.001$, **** $p < 0.0001$.

SUPPLEMENTARY FIGURE 6: RELATED TO FIGURE 4

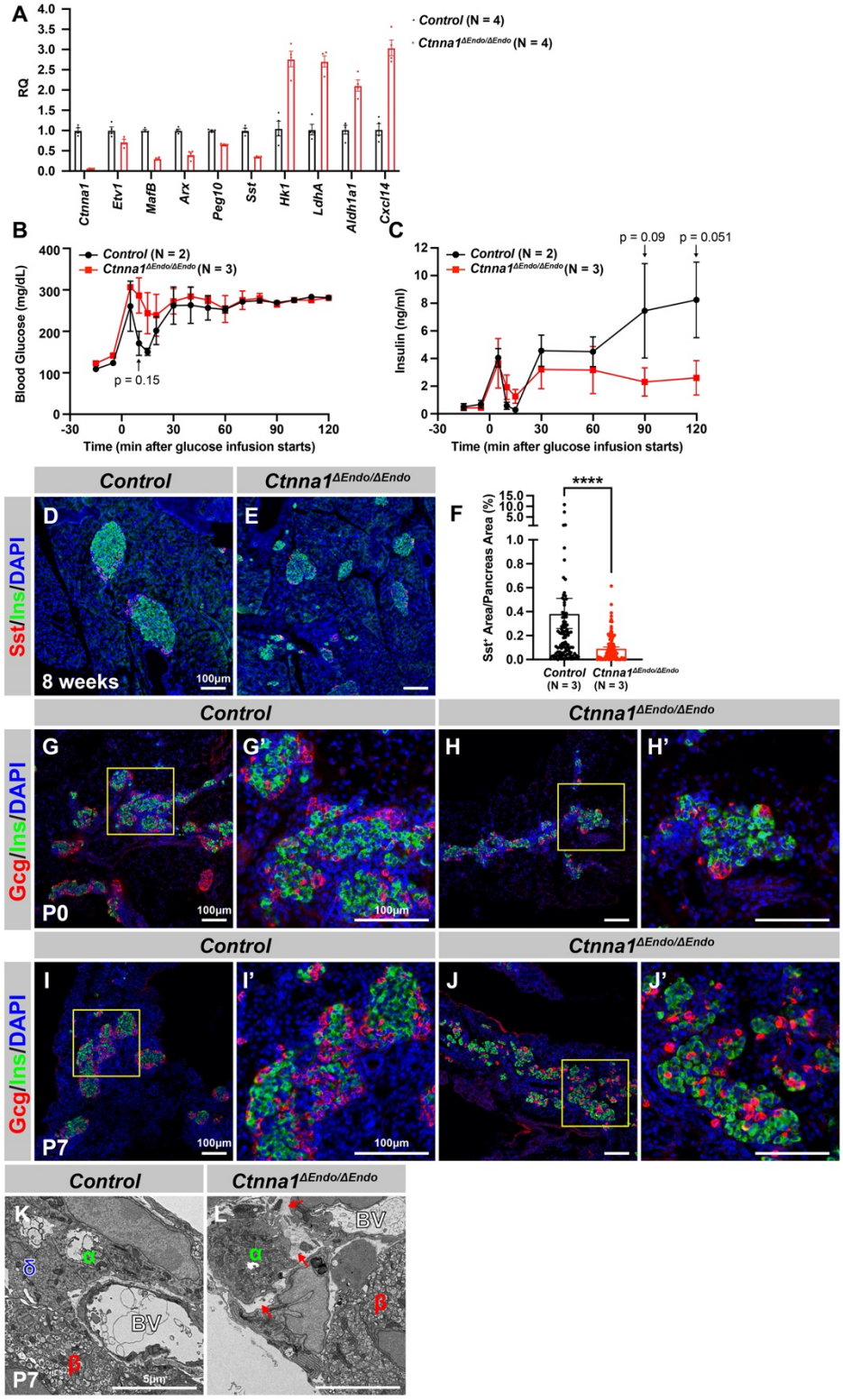

871

872 **Figure S6. Ctnna1 is required for proper islet functionality and normal islet aggregation.**
873 **Related to Figure 4.**
874 (A) Quantification of selected differentially expressed genes involved in islet functional maturation
875 using real-time qPCR analysis in *Ctnna1*$^{\Delta Endo/\Delta Endo}$ islets and compared to controls. The relative
876 quantification of gene expression levels was determined using the $2^{-\Delta\Delta Ct}$ method and is reported
877 as a RQ value relative to the control group. The genes selected for validation were chosen based
878 on their known roles in islet function and maturation.
879 (B-C) Whole-blood glucose (B; mg/dL) and Insulin secretion (C; ng/ml) during 120 min in
880 euglycemic clamp experiments in 5-h-fasted, surgically catheterized control and *Ctnna1*$^{\Delta Endo/\Delta Endo}$
881 mice at 8 weeks of age. At 5-15 minutes after glucose infusion, *Ctnna1*$^{\Delta Endo/\Delta Endo}$ mice showed
882 slightly elevated glucose levels compared to controls (P=0.15). The amount of insulin secretion
883 in *Ctnna1*$^{\Delta Endo/\Delta Endo}$ mice decreased at 90 and 120 minutes after glucose infusion (P=0.09 and
884 0.051, respectively). These results suggest that *Ctnna1*$^{\Delta Endo/\Delta Endo}$ mice may have impaired glucose
885 metabolism and insulin secretion.
886 (D-E) Immunofluorescence staining for Sst (red), Ins (green), and DAPI (blue) in pancreas
887 sections of 8 weeks old control and *Ctnna1*$^{\Delta Endo/\Delta Endo}$ mice. (F) Quantification of the Sst^+ area
888 relative to the total pancreas area shows a decrease in the number of Sst^+ cells in *Ctnna1*$^{\Delta Endo/\Delta Endo}$
889 mice compared with their control.
890 (G-J) Immunofluorescence staining for Gcg (red), Ins (green), and DAPI (blue) in pancreas
891 sections of P0 (G and H) and P7 (I and J) control and *Ctnna1*$^{\Delta Endo/\Delta Endo}$ mice. The fields
892 demarcated by yellow boxes in (G-J) are shown at higher magnification in (G'-J').
893 (K-L) Transmission electron microscope images of P7 control (K) and *Ctnna1*$^{\Delta Endo/\Delta Endo}$
894 (L) endocrine areas. Red arrows indicate detachment of an α-cell from an islet aggregate.
895
896 RQ, Relative quantification; Sst, Somatostatin; Gcg, Glucagon; Ins, Insulin; DAPI, 4',6-diamidino-
897 2-phenylindole; P0, postnatal day 0; P7, postnatal day 7; BV, blood vessels
898 Data are shown as mean ± SEM. * $p < 0.05$, **** $p < 0.0001$.

FIGURE 5

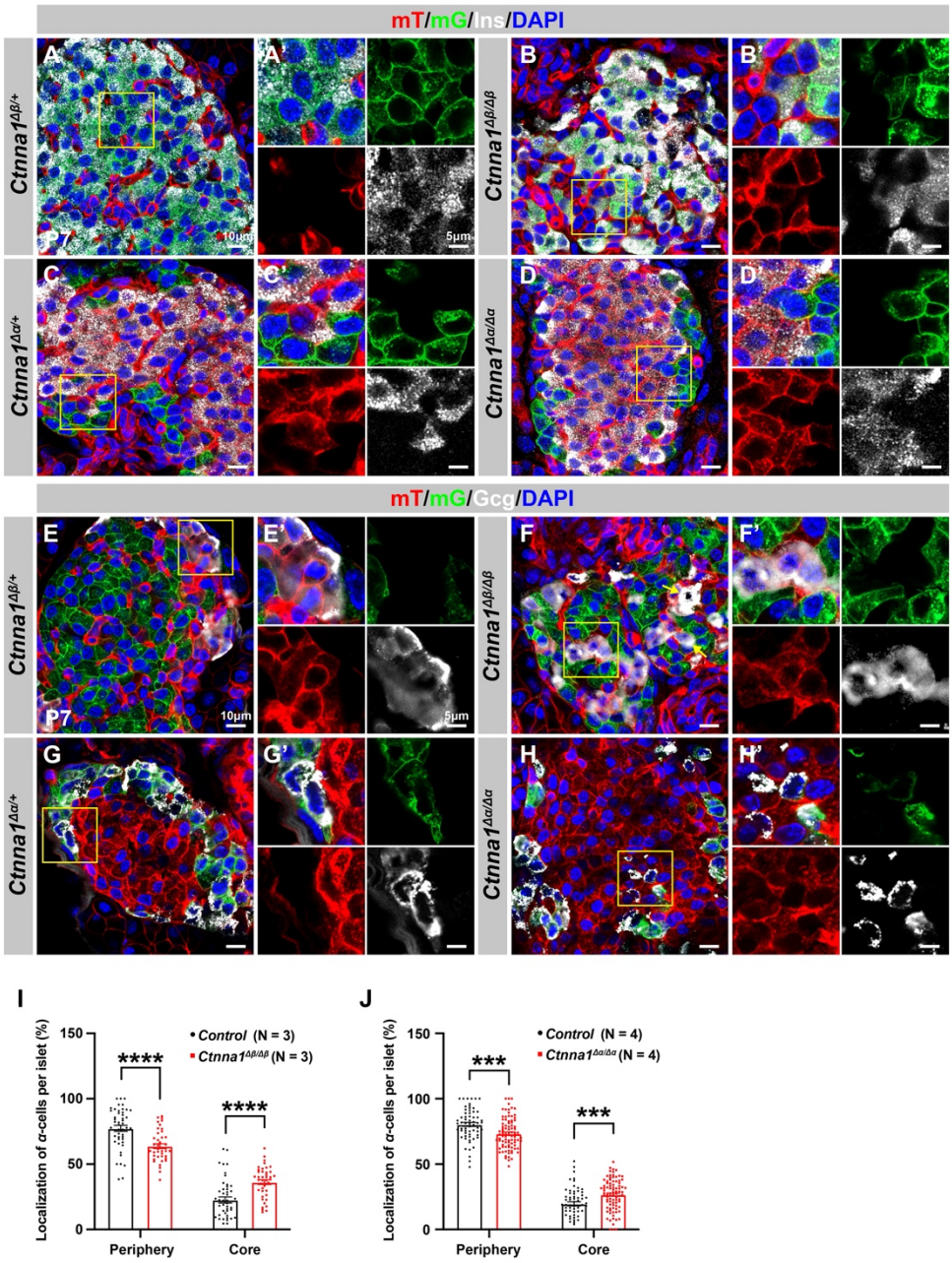
mT/mG/Ins/DAPI
Ctnna1Δβ/+
Ctnna1Δβ/Δβ
Ctnna1Δα/+
Ctnna1Δα/Δα
A
A'
B
B'
C
C'
D
D'
P7
10μm
5μm
mT/mG/Gcg/DAPI
E
E'
F
F'
G
G'
H
H'
I
Localization of α-cells per islet (%)
Control (N = 3)
Ctnna1Δβ/Δβ (N = 3)
****
Periphery
Core
J
Control (N = 4)
Ctnna1Δα/Δα (N = 4)
***

899

900 **Figure 5. Loss of Ctnna1 in α- and β-cells leads to disrupted islet architecture**
901 (A-H) Airyscan images of immunofluorescence staining for Ins (A-D), Gcg (E-H), and DAPI in
902 pancreas sections of P7 mT/mG reporter mice: Heterozygous *Ctnna1*$^{\Delta\beta/+}$ (A,E), homozygous
903 *Ctnna1*$^{\Delta\beta/\Delta\beta}$ (B,F), heterozygous *Ctnna1*$^{\Delta\alpha/+}$ (C,G), and homozygous *Ctnna1*$^{\Delta\alpha/\Delta\alpha}$ (D,H). The yellow
904 arrows in (F) showing α-cells in the islet core in *Ctnna1*$^{\Delta\beta/\Delta\beta}$ mice. The fields demarcated by yellow
905 boxes are shown at higher magnification with individual color channels in the side panels.
906 (I-J) Quantification of α-cell localization in the islets of *Ctnna1*$^{\Delta\beta/\Delta\beta}$ (I) and *Ctnna1*$^{\Delta\alpha/\Delta\alpha}$ (J) mice.
907 Compared to controls, *Ctnna1*$^{\Delta\beta/\Delta\beta}$ and *Ctnna1*$^{\Delta\alpha/\Delta\alpha}$ mice exhibit a reduction in peripherally located
908 α-cells and an increase in core-located α-cells. These results suggest that the loss of Ctnna1 in
909 α- and β-cells affects the organization and localization of α-cells within the islet.
910
911 Gcg, Glucagon; DAPI, 4',6-diamidino-2-phenylindole; Ins, Insulin; P7, postnatal day 7
912 Data are shown as mean ± SEM. *** $p < 0.001$, **** $p < 0.0001$.

SUPPLEMENTARY FIGURE 7: RELATED TO FIGURE 5

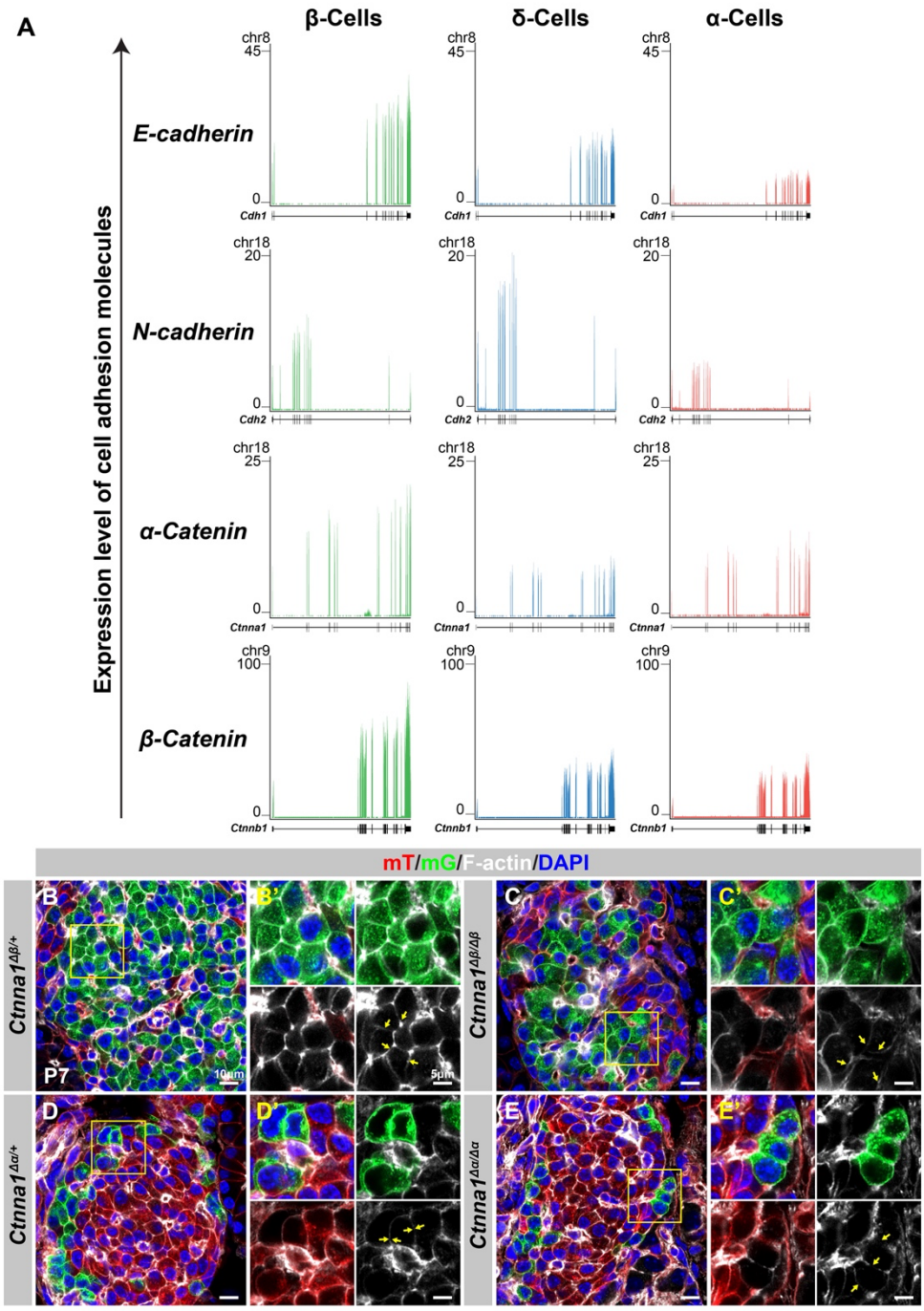

913

914 **Figure S7. Differential cell-cell adhesion in endocrine cells. Related to Figure 5.**
915 (A) Genome viewer plots comparing expression levels of adhesion molecules in α-, β-, and δ- cell
916 transcriptomes (DiGruccio et al., 2016).
917 (B-E) Airyscan images of immunofluorescence staining of P7 mT/mG reporter mice stained for F-
918 actin and DAPI in (B) heterozygous *Ctnna1*$^{\Delta\beta/+}$, (C) homozygous *Ctnna1*$^{\Delta\beta/\Delta\beta}$, (D) heterozygous
919 *Ctnna1*$^{\Delta\alpha/+}$, and (E) homozygous *Ctnna1*$^{\Delta\alpha/\Delta\alpha}$ mice. Fields demarcated by yellow boxes in B-E are
920 shown at higher magnification with individual color channels in B'-E' side panels. Yellow arrows
921 indicate expression of F-actin in (B,C) and β- (D,E) α-cells.
922
923 DAPI, 4',6-diamidino-2-phenylindole; P7, postnatal day 7
924
925

FIGURE 6

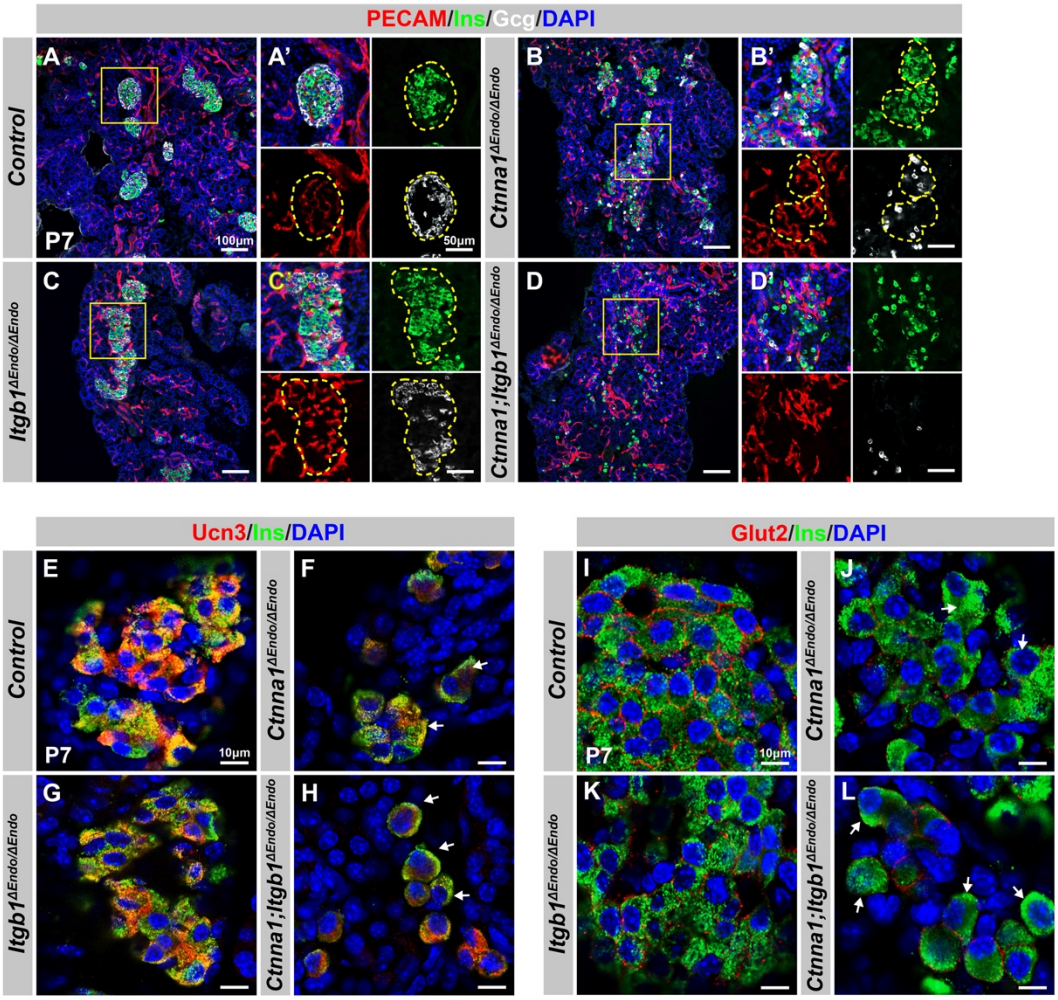
PECAM/Ins/Gcg/DAPI
Control
Itgb1ΔEndo/ΔEndo
Ctnna1ΔEndo/ΔEndo
Ctnna1;Itgb1ΔEndo/ΔEndo
A
A'
B
B'
C
C'
D
D'
P7
100µm
50µm
Ucn3/Ins/DAPI
Glut2/Ins/DAPI
E
F
G
H
I
J
K
L
10µm

926

927 **Figure 6. Disruption of cell-ECM and/or cell-cell adhesion results in abnormal islet vascular**
928 **architecture, endocrine cell aggregation, and decreased expression of β-Cell maturation**
929 **markers at postnatal day 7.**
930 (A-D) Immunofluorescence staining of PECAM, Ins, Gcg, and DAPI in P7 (A) control, (B)
931 *Ctnna1*$^{\Delta Endo/\Delta Endo}$, (C) *Itgb1*$^{\Delta Endo/\Delta Endo}$, and (D) *Ctnna1; Itgb1*$^{\Delta Endo/\Delta Endo}$ mice. Fields demarcated by
932 yellow boxes in A-D are shown at higher magnification in A'-D' side panels. Individual islet shape
933 is outlined by dashed yellow lines in A'-C'. Endocrine cells are suspended and scattered
934 throughout the pancreas of *Ctnna1; Itgb1*$^{\Delta Endo/\Delta Endo}$ mice.
935 (E-L) Airyscan images of immunofluorescence staining for Ucn3, Glut2, Ins, and DAPI in P7 (E,I)
936 control, (F,J) *Ctnna1*$^{\Delta Endo/\Delta Endo}$, (G,K) *Itgb1*$^{\Delta Endo/\Delta Endo}$, and (H,L) *Ctnna1; Itgb1*$^{\Delta Endo/\Delta Endo}$ mice.
937 Arrows indicate reduced expression of Ucn3 or Glut2 in β-cells of the mutant mice.
938
939 PECAM, Platelet endothelial cell adhesion molecule-1; Ins, Insulin; Gcg, Glucagon; DAPI, 4',6-
940 diamidino-2-phenylindole; Ucn3, Urocortin 3; Glut2, Slc2a2; P7, postnatal day 7

SUPPLEMENTARY FIGURE 8: RELATED TO FIGURE 6

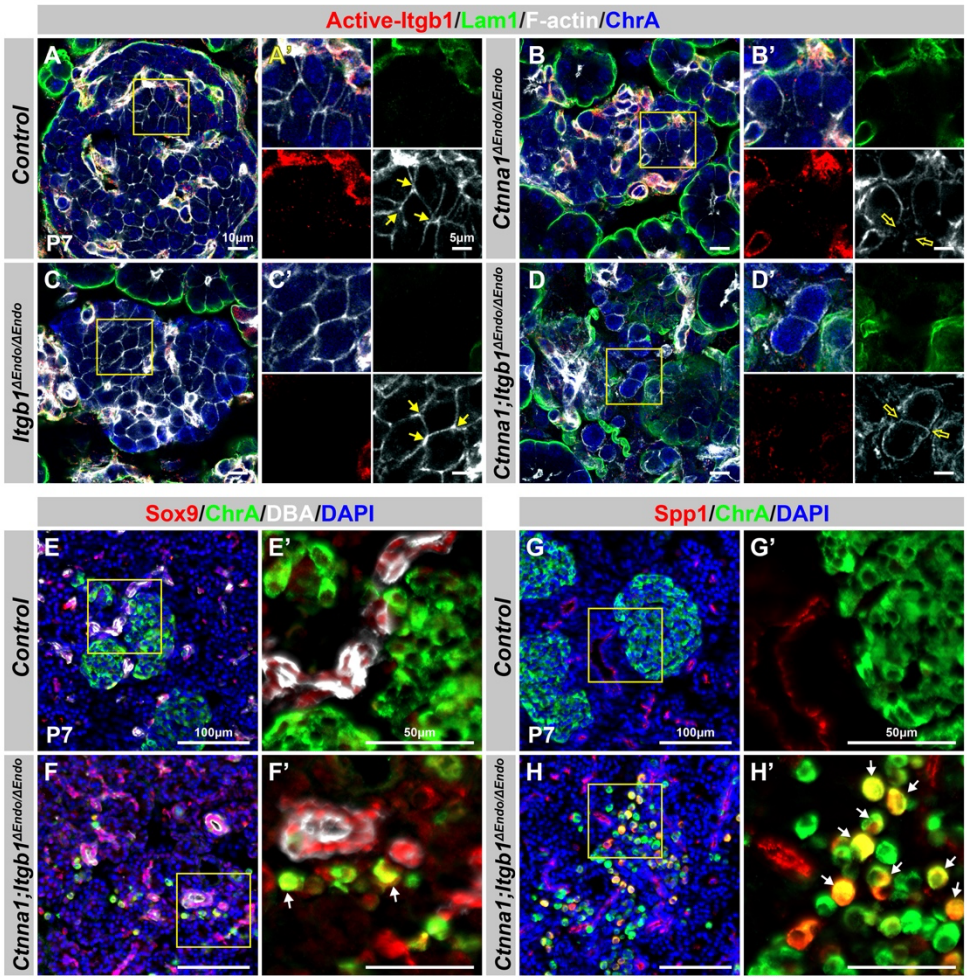

941

942 **Figure S8. Aberrant endocrine cell clustering and upregulation of islet progenitor markers**
943 **upon disruption of cell adhesion. Related to Figure 6.**
944 (A-D) Airyscan images showing immunofluorescence staining for active-Itgb1, Lam1, F-actin, and
945 ChrA in pancreas sections from (A) control, (B) *Ctnna1*$^{\Delta Endo/\Delta Endo}$, (C) *Itgb1*$^{\Delta Endo/\Delta Endo}$, and (D)
946 *Ctnna1; Itgb1*$^{\Delta Endo/\Delta Endo}$ mice at P7. The yellow boxes in A-D indicate the fields shown at higher
947 magnification in A'-D' side panels. The yellow arrows point to F-actin expression in endocrine
948 cells. The *Ctnna1*$^{\Delta Endo/\Delta Endo}$ (B') and *Ctnna1; Itgb1*$^{\Delta Endo/\Delta Endo}$ (D') islet cells exhibit a round cell
949 shape and reduced F-actin-enriched junctional structures.
950 (E-H) Immunofluorescence staining for endocrine cell marker ChrA (green), ductal marker DBA
951 (white in E, F), and progenitor markers Sox9 (red in E, F) and Spp1 (red in G, H) on pancreas
952 sections from control (E, G) and *Ctnna1; Itgb1*$^{\Delta Endo/\Delta Endo}$ (F, H) mice at P7. The yellow boxes in
953 (E-H) indicate the fields shown at higher magnification in (E'-H') side panels. Compared to
954 controls, in which ChrA^{+} endocrine cells do not express progenitor markers Sox9 and Spp1 (E'
955 and G'), a subpopulation of ChrA^{+} endocrine cells in the islets of *Ctnna1; Itgb1*$^{\Delta Endo/\Delta Endo}$ mice
956 exhibit upregulated expression of Sox9 and Spp1 (yellow cells indicated by arrows in F' and H').
957
958 Lam1, Laminin1; ChrA; Chromogranin A; P7, postnatal day 7; DBA, *Dolichos biflorus* agglutinin

FIGURE 7

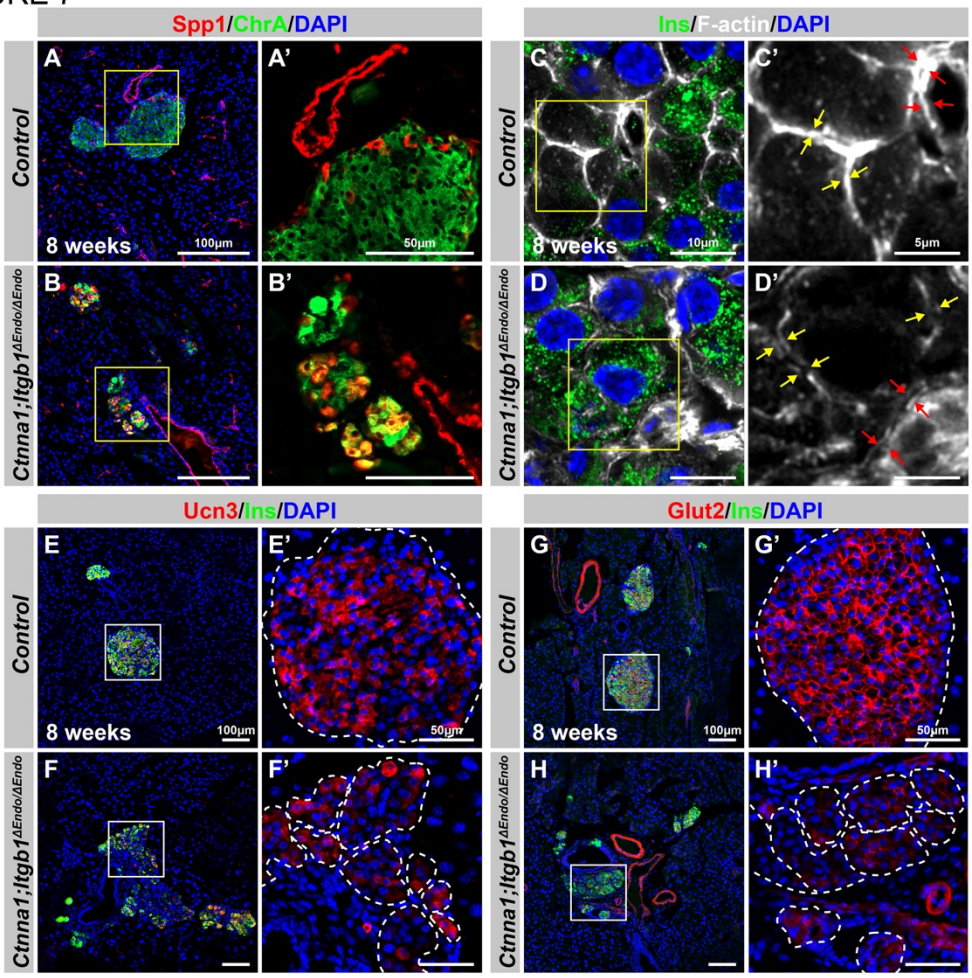
Spp1/ChrA/DAPI
Ins/F-actin/DAPI
Control
Ctnna1;Itgb1ΔEndo/ΔEndo
A
A'
B
B'
C
C'
D
D'
8 weeks
100µm
50µm
10µm
5µm
Ucn3/Ins/DAPI
Glut2/Ins/DAPI
E
E'
F
F'
G
G'
H
H'

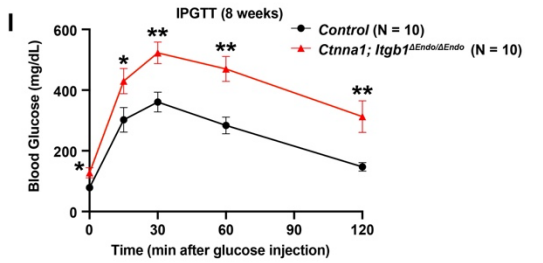
I
IPGTT (8 weeks)
Control (N = 10)
Ctnna1; Itgb1ΔEndo/ΔEndo (N = 10)
Blood Glucose (mg/dL)
Time (min after glucose injection)
0
200
400
600
0
30
60
90
120
*
**

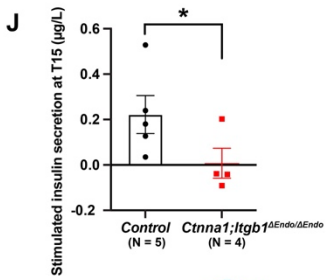
J
Stimulated insulin secretion at T15 (µg/L)
0.6
0.4
0.2
0.0
-0.2
*
Control
(N = 5)
Ctnna1;Itgb1ΔEndo/ΔEndo
(N = 4)

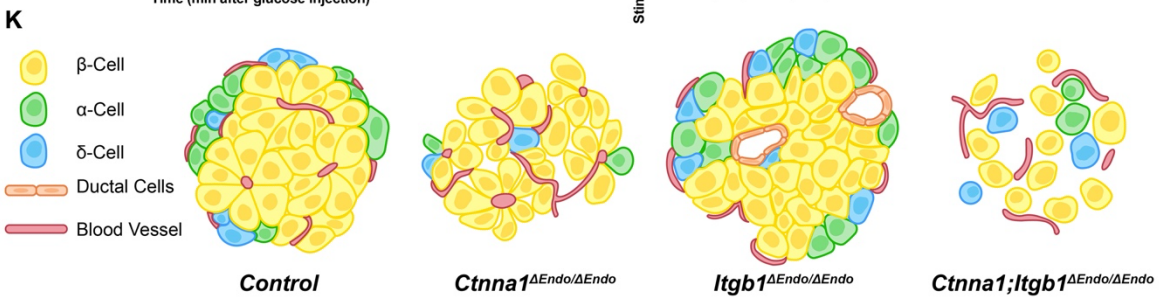
K
β-Cell
α-Cell
δ-Cell
Ductal Cells
Blood Vessel
Control
Ctnna1ΔEndo/ΔEndo
Itgb1ΔEndo/ΔEndo
Ctnna1;Itgb1ΔEndo/ΔEndo

959

Figure 7. Abnormal islet aggregation, mis-regulation of β-Cell maturation markers, and insulin secretion defects persist in *Ctnna1; Itgb1$^{\Delta Endo/\Delta Endo}$* mice into adulthood.

(A-B) Immunofluorescence staining for endocrine cell marker ChrA and progenitor marker Spp1 on pancreas sections from control (A) and *Ctnna1; Itgb1$^{\Delta Endo/\Delta Endo}$* (B) mice at 8 weeks old. The yellow boxes in A,B indicate the fields shown at higher magnification in A',B' side panels. In the islets of *Ctnna1; Itgb1$^{\Delta Endo/\Delta Endo}$* mice, a subpopulation of ChrA^{+} endocrine cells expresses progenitor markers Spp1 (yellow cells in B and B').

(C-D) Airyscan images of immunofluorescence staining for Ins, F-actin and DAPI in pancreatic sections from 8-week-old control and *Ctnna1; Itgb1$^{\Delta Endo/\Delta Endo}$* mice are shown. In control islets (C,C'), the F-actin assemblies appear aligned with cell membranes and condensed in cellular junctions, as indicated by the yellow and red arrows, respectively. In contrast, diffused distribution of F-actin (red arrows in D') and separation of F-actin assemblies (yellow arrows in D') between Ins^{+} β-cells are observed in the *Ctnna1; Itgb1$^{\Delta Endo/\Delta Endo}$* mice.

(E-F) Immunofluorescence staining of Ucn3, Ins, and DAPI in pancreatic sections of 8 weeks old (E) control and (F) *Ctnna1; Itgb1$^{\Delta Endo/\Delta Endo}$* mice. Fields demarcated by white boxes in E and F are shown at higher magnification in E' and F', and individual islet shape is outlined by dashed white lines. The reduction of Ucn3 expression persists in adult *Ctnna1; Itgb1$^{\Delta Endo/\Delta Endo}$* mice.

(G-H) Immunofluorescence staining of Glut2, Ins, and DAPI in 8 weeks old (G) control and (H) *Ctnna1; Itgb1$^{\Delta Endo/\Delta Endo}$* mouse pancreas. Fields demarcated by white boxes in G and H are shown at higher magnification in G' and H', and individual islet shape is outlined by dashed white lines. The reduction of Glut2 expression persists in adult *Ctnna1; Itgb1$^{\Delta Endo/\Delta Endo}$* mice.

(I-J) Intraperitoneal glucose tolerance test was performed on 8-week-old mice (I), and glucose-stimulated insulin secretion was measured at T15 in 20-38 -week-old mice (J) from control and *Ctnna1; Itgb1$^{\Delta Endo/\Delta Endo}$* groups. *Ctnna1; Itgb1$^{\Delta Endo/\Delta Endo}$* mice exhibited severe glucose intolerance and defects in insulin secretion.

(K) Graphical summary of the islet phenotypes observed after disruption of cell-cell and cell-ECM adhesion.

Ins, Insulin; ChrA, Chromogranin A; Spp1, Secreted Phosphoprotein 1; Ucn3, Urocortin 3; IPGTT, intraperitoneal glucose tolerance test

Data are shown as mean ± SEM. * $p < 0.05$ and ** $p < 0.01$.

992 **EXPERIMENTAL MODEL AND SUBJECTS DETAILS**
993
994 **Mouse Strains**
995 All animal experiments described herein were approved by the City of Hope Institutional Animal
996 Care and Use Committees. Mice carrying *Ngn3-Cre* (Schonhoff et al., 2004), *R26*$^{mT/mG}$
997 (Muzumdar et al., 2007), *Gcg-iCre* (Shiota et al., 2017), *Itgb1*^{flox} (Raghavan et al., 2000), *Ctnna1*^{flox}
998 (Vasioukhin et al., 2001), *Ins-Cre* (Thorens et al., 2015), *R26*$^{mT/mG}$ (Muzumdar et al., 2007),
999 *R26*^{EYFP} (Srinivas et al., 2001), and *Ucn3-cre* (Harris et al., 2014) alleles have been previously
1000 described. Additional information for the mouse lines used in this study is listed in Key Resources
1001 Table.
1002
1003 **METHOD DETAILS**
1004
1005 **Whole Mount Immunofluorescence (WMIF)**
1006 A standard whole mount staining protocol was utilized to analyze pancreas three-dimensional (3D)
1007 morphology, as previously described (Maldonado et al., 2020). Briefly, pancreas tissue was
1008 dissected and fixed overnight in 4% paraformaldehyde (PFA). The tissue was dehydrated with
1009 serial methanol washes, bleached with a Dent's Bleach solution, and rehydrated using an inverse
1010 series of methanol washes. Samples were blocked followed by incubation with primary antibodies
1011 for Platelet endothelial cell adhesion molecule-1 (PECAM), Chromogranin A (ChrA), and Secreted
1012 Phosphoprotein 1 (Spp1). Samples were then washed in a 0.15% triton-X-PBS solution and
1013 stained with secondary antibodies overnight. Following additional washes with 0.15% triton-X-
1014 PBS, samples were fixed with 4% PFA, and dehydrated with serial ethanol washes. Finally,
1015 samples were immersed in a BABB clearing solution (two parts benzyl benzoate and one part
1016 benzyl alcohol) and imaged using a Zeiss LSM880 confocal microscope.
1017
1018 **Confocal Microscopy**
1019 All images were collected with a Zeiss LSM880 confocal microscope equipped with a 10X 0.45NA
1020 plan apochromat objective at 2X magnification, as standard for AiryscanFast collection. All tiled
1021 Z-stacks were acquired in AiryscanFast mode, the acquisition method set to Z-stack (per channel),
1022 and with a 2.0 micron step size. Scans were conducted using 405nm, 488nm, 561nm, and 633nm
1023 laser lines, and emissions were collected using standard Airyscan filters and the Airyscan detector,
1024 in Zen Black 2.3 SP1 (Carl Zeiss). Final voxel sizes were 0.22x0.22x1.98 microns, and no digital
1025 gain or detector offset was used. Detector gains and laser intensities were consistent across all
1026 samples.
1027
1028 **Image Segmentation/Analysis**
1029 Data sets were first Airyscan processed in Zen Black using the "Auto" setting using a 2D sample
1030 image as a base for Batch mode. After processing, the files were converted to IMS format and
1031 analyzed in Imaris 9.5 (Bitplane). Analysis consisted of manually selecting thresholds that could
1032 be consistently applied between samples, and best fit the biology. Due to variations in the depth
1033 of the sample, amount of tissue the light had to pass through, and orientation, thresholds were
1034 chosen which most accurately represented the objects being analyzed. The ducts were first
1035 segmented using a "Surface" with a 2.00-micron surface grain size, and a fixed threshold. We

1036 limited the analysis to areas where ducts were present by segmenting the duct channel a second
1037 time (again as a Surface) with a grain size of 10 microns and a much lower threshold, generating
1038 a “bubble” area of interest around the ducts. Within this volume, endocrine positive staining was
1039 then segmented as another surface and its distance from the ducts quantified using the median
1040 value of the distance transform from the surface of the original ducts. Any endocrine cells
1041 contained entirely or mostly within the ducts were considered to have a distance of zero from the
1042 ducts.
1043
1044 **Immunofluorescence (IF)**
1045 Pancreas tissues were collected from littermate control and mutant mice, ensuring consistency in
1046 the sample source. Immunofluorescence staining was performed as previously described (Shih
1047 et al., 2007). Briefly, pancreata were fixed in 4% paraformaldehyde in PBS, equilibrated in 30%
1048 sucrose in PBS, and cryoembedded in Tissue-Tek OCT. To ensure the reliability and accuracy of
1049 the findings, we used littermate control and mutant mice, collecting and processing their pancreas
1050 samples concurrently. This included fixing and embedding the samples into the same cryo-block,
1051 sectioning, and preparing them for immunofluorescence staining on the same slide. This process
1052 ensured identical staining conditions for all samples. Samples were then sectioned at 10 µm
1053 intervals from the same cryo-block, facilitating identical staining conditions for all samples. For
1054 immunofluorescence staining, sections were blocked for 1 hour before the addition of primary
1055 antibodies diluted in the same buffer. Following washes, secondary antibodies, diluted in blocking
1056 buffer, were applied to sections and stained for 2 hours at room temperature. The respective
1057 dilutions of primary and secondary antibodies are noted in the Key Resources Table.
1058
1059 Images were taken on a Zeiss Axio-Observer-Z1 microscope with Apotome, and figures were
1060 created in Adobe Photoshop/Illustrator CC2020. Morphometric analyses were conducted using
1061 Image-Pro Premier v.9.2 and Qupath software, available at https://qupath.github.io. High
1062 resolution image acquisition was achieved with a Zeiss LSM900 confocal microscope with
1063 Airyscan. For images intended for direct comparison, the exposure time was kept constant, and
1064 changes in digital gain were avoided to prevent distortion of results. Upon image acquisition, linear
1065 adjustment processing was applied uniformly across all comparable samples. These adjustments
1066 were made using a linear display with Min/Max rescaling. This adjustment approach was to
1067 carefully balance avoiding oversaturation while preserving the accuracy of marker
1068 expressions. This approach ensures that the full data range is properly utilized, optimizing the full
1069 range of possible intensity values. Specifically, the darkest pixel in the image is adjusted to black
1070 (minimum value), the brightest pixel to white (maximum value), and all other pixels are rescaled
1071 based on these new extremes.
1072
1073 **α-cell Localization Analysis**
1074 The islets were imaged from three serial sections per mouse, taken at 150 µm (P7) or 200 µm (8
1075 weeks) intervals. Manual cell counting was performed using QuPath (version 0.2.3). Islets with a
1076 minimum of 40 endocrine cells and at least 10 α-cells were included in the analysis. At the
1077 postnatal stage, α-cell localization within the islet was determined according to previously
1078 described criteria (Adams et al., 2018). Peripheral α-cells were defined as those within the first
1079 two layers, while α-cells in any layers beyond the first two were considered to be in the core.

1080
1081 **Intra Peritoneal Glucose Tolerance Test (IPGTT)**
1082 6 to 16 weeks old or 6 to 12 months old mice were fasted for 6-16 hours. Basal blood glucose
1083 was measured, and mice were injected intraperitoneally (i.p.) with 2 mg/g body weight dextrose
1084 solution. Blood glucose was measured at 15, 30, 60, 90 and 120 minutes after glucose challenge.
1085 The experiments were performed by the Comprehensive Metabolic Phenotyping (CMP) Core at
1086 City of Hope.
1087
1088 **Insulin secretion *in vivo***
1089 The β-cell function was assessed by quantifying insulin secretion *in vivo* with hyperglycemic
1090 clamps. Surgical procedures have been described in detail previously(Ayala et al., 2011; Berglund
1091 et al., 2008). Briefly, mice were anesthetized with isoflurane, and the carotid artery and jugular
1092 vein were catheterized. Free catheter ends were tunneled under the skin to the back of the neck
1093 and externalized with a MASA™ (Mouse Antenna for Sampling Access), which permits arterial
1094 sampling from an indwelling catheter in conscious mice without handling stress. Mice were
1095 individually housed and allowed to recover for 4 days during which body weight returned to
1096 within ∼10% of presurgical body weight.
1097
1098 For the hyperglycemic clamps, mice were fasted for 5 h and connected to a swivel. Saline-washed
1099 erythrocytes were infused (5–6 µl/min) during the experimental period to prevent a >5% fall in
1100 hematocrit. Blood samples were collected from the arterial catheter in tubes containing EDTA
1101 and centrifuged, and plasma was stored at −20°C until analyzed. At t = 0 min, mice received a
1102 priming glucose infusion rate (GIR, 100 mg/kg/min) for 2 min to stimulate first-phase insulin
1103 secretion. The GIR was then adjusted to achieve and maintain blood glucose at ∼15.0 mmol/l.
1104 Blood glucose (5 µl) was measured at t = −15, −5, 5, 10, 15, and 20 min and then every 10 min
1105 until t = 120 min with an Alpha Trak glucometer (Abbott Laboratories, Abbott Park, IL, USA).
1106 Larger blood samples (100 µl) to measure plasma insulin were taken at various timepoints.
1107
1108 **Isolation of Mouse Pancreatic Islets**
1109 Pancreatic islets were isolated as previously described (Taylor et al., 2013). Briefly, mouse
1110 pancreatic islets were isolated using 2.5 mg/ml collagenase (Sigma Aldrich) as the digestion
1111 method. Islets were collected under a stereomicroscope and allowed to recover overnight in
1112 PIM(R)® 32A (Prodo Labs) medium with 5% HSA, Gentamicin-AmphotericinB, and 5.8 mmol/L
1113 glucose.
1114
1115 **RNA-Sequencing (RNA-seq)**
1116 Total RNA was isolated using the RNeasy Micro Kit (Qiagen) with 10 to 30 isolated islets and
1117 processed per manufacturer's instructions. cDNA libraries were prepared using the KAPA RNA
1118 HyperPrep Kit with RiboErase (HMR) according to the manufacturer's instructions. Libraries were
1119 subjected to high-throughput sequencing on Illumina HiSeq 2500 (50 bp, single-ended) and
1120 subsequent data analysis was completed by the Integrative Genomics Core at City of Hope. For
1121 sequence alignment and gene counts, RNA-Seq reads were trimmed to remove sequencing
1122 adapters using Trimmomatic (Bolger et al., 2014) and polyA tails using FASTP (Chen et al., 2018).
1123 The processed reads were mapped back to the mouse genome (mm10) using STAR software (v.

1124 020201) (Dobin et al., 2013). The featureCount software was applied to generate the count matrix,
1125 with default parameters (Liao et al., 2019). Between two sets of samples (Control vs Mutant),
1126 differential expression analysis was conducted, in R, by adjusting read counts to normalized
1127 expression values using TMM normalization method and by correcting batch effects using a
1128 design matrix (Robinson et al., 2010). Genes with an FDR-adjusted p-value less than 0.05 and
1129 with a fold change (FC) greater than 2 or less than 0.5 were considered as significant up- and
1130 down-regulated genes, respectively. Pathway analysis was conducted using DAVID (v. 6.8)
1131 (Huang da et al., 2009a, b) and GSEAPreranked algorithm using GSEA Desktop program in Java
1132 (Subramanian et al., 2005). The former requires a list of up- and down-regulated genes, while the
1133 latter a ranked list of whole genes according to their log2 fold change and p-values. Raw data and
1134 processed data files were available at the GEO database:
1135 (GSE153187, https://www.ncbi.nlm.nih.gov/geo/query/acc.cgi?acc=GSE153187).
1136 (GSE190788, https://www.ncbi.nlm.nih.gov/geo/query/acc.cgi?acc=GSE190788).
1137
1138 **Quantitative real-time PCR (qPCR)**
1139 RNA extraction and purification were performed using the RNeasy Micro Kit (QIAGEN) in
1140 accordance with the manufacturer's protocol. The quality and quantity of the total RNA were
1141 assessed using a Bioanalyzer 2100 (Agilent Technologies). Samples with an RNA integrity
1142 number (RIN) of at least 6 were used for cDNA synthesis with the SuperScript™ First-Strand
1143 Synthesis SuperMix for qRT-PCR (Invitrogen). Real-time PCR was conducted using PowerUp™
1144 SYBR™ Green Master mix (Applied Biosystems) in a QuantStudio 6 Flex machine (Applied
1145 Biosystems). Each reaction contained 1 ng cDNA (total RNA equivalent). Relative mRNA
1146 expression levels were calculated by normalizing target genes to *Cyclophilin A* (*Ppia*) as an
1147 internal control. All primers were designed using the CDS of the target genes by the PrimerBank
1148 online tool (https://pga.mgh.harvard.edu/primerbank/).
1149
1150 **Aggregation Assay**
1151 Neonatal *Ngn3-Cre; R26mT/mG; Itgb1*$^{+/f}$ (control) or *Ngn3-Cre; R26mT/mG; Itgb1*$^{f/f}$ (mutant)
1152 pancreata were dissociated into a single cell suspension using TrypLE (Thermo Fisher).
1153 Enzymatic activity was neutralized using FACS buffer (10% fetal bovine serum (FBS) and 2mM
1154 EDTA in CMRL media). Cells were passed through a 40 µm cell strainer and DAPI was used to
1155 stain dead cells prior to FACS. Prior to cell seeding, 96-well round bottom plates were coated with
1156 either bovine serum albumin (BSA; no ECM) or Matrigel and fibronectin (+ECM). 3000 cells per
1157 well were added into no ECM or +ECM wells and cultured for 48 hours.
1158
1159 ***Ex Vivo* Pancreas Explants**
1160 Pancreas explants are described previously (Shih and Sander, 2014). After 24 hours of culture,
1161 the explants were placed on the microscope stage in 37 °C culture chambers with a controlled
1162 atmosphere of humidified 5% CO_2. Time-lapse imaging was performed using a Zeiss LSM880
1163 inverted confocal microscope with a C-Apochromat 20×/0.75 objective lens. Explants were
1164 optically sectioned every 2.5 µm in a 512 × 512 format with up to 80 µm Z-stacks every 10 min
1165 for 72 hours. Images were acquired with Zen software and then reconstructed in 3D with Imaris
1166 9.5 (Bitplane) software. The contrast was adjusted and selected optical planes or *z*-projections of
1167 sequential optical sections were used to assemble time-lapse movies.

1168
1169 **Electron Microscopy Sample Preparation**
1170 Sample blocks were prepared following the NCMIR protocol (T.J. Deerinck, 2010). Briefly, small
1171 pieces (1~2 mm^3) of mouse pancreatic tissues were dissected and immediately fixed in 0.2M
1172 cacodylate buffer pH7.4 containing 2.5% glutaraldehyde and 2% paraformaldehyde with 3mM
1173 calcium chloride. After primary aldehyde fixation the samples were rinsed in 0.15M sodium
1174 cacodylate pH7.4 containing 2mM calcium chloride and post-fixed in 1.5% potassium
1175 ferrocyanide-reduced 2% osmium tetroxide in 0.15M cacodylate buffer for 1 hour. Tissue was
1176 then rinsed in distilled water and treated with 0.1% aqueous thiocarbohydrazide for 20 min. After
1177 further rinsing in distilled water the tissue was again treated with 2% osmium tetroxide for 30 min,
1178 rinsed in distilled water, dehydrated in an ethanol series, and infiltrated with Durcupan ACM resin.
1179 Ultra-thin sections (70 nm thick) were acquired by ultramicrotomy and examined on a FEI Tecnai
1180 12 transmission electron microscope equipped with a Gatan OneView CMOS camera.
1181
1182 **Statistics**
1183 The statistical analysis was performed using GraphPad Prism. To compare groups, one-way
1184 analysis of variance (ANOVA) and a two-tailed student's t-test were utilized, unless otherwise
1185 specified. Each group was evaluated using a minimum of three independent measurements.
1186 Unless stated otherwise, all data are presented as mean ± standard error of the mean (SEM).
1187

REFERENCES

Adams, M.T., and Blum, B. (2022). Determinants and dynamics of pancreatic islet architecture. Islets *14*, 82-100.

Adams, M.T., Dwulet, J.M., Briggs, J.K., Reissaus, C.A., Jin, E., Szulczewski, J.M., Lyman, M.R., Sdao, S.M., Kravets, V., Nimkulrat, S.D*., et al.* (2021). Reduced synchroneity of intra-islet Ca(2+) oscillations in vivo in Robo-deficient beta cells. Elife *10*.

Adams, M.T., Gilbert, J.M., Hinojosa Paiz, J., Bowman, F.M., and Blum, B. (2018). Endocrine cell type sorting and mature architecture in the islets of Langerhans require expression of Roundabout receptors in beta cells. Sci Rep *8*, 10876.

Alto, L.T., and Terman, J.R. (2017). Semaphorins and their Signaling Mechanisms. Methods Mol Biol *1493*, 1-25.

Arrojo e Drigo, R., Ali, Y., Diez, J., Srinivasan, D.K., Berggren, P.O., and Boehm, B.O. (2015). New insights into the architecture of the islet of Langerhans: a focused cross-species assessment. Diabetologia *58*, 2218-2228.

Ayala, J.E., Bracy, D.P., Malabanan, C., James, F.D., Ansari, T., Fueger, P.T., McGuinness, O.P., and Wasserman, D.H. (2011). Hyperinsulinemic-euglycemic clamps in conscious, unrestrained mice. J Vis Exp.

Balboa, D., Barsby, T., Lithovius, V., Saarimaki-Vire, J., Omar-Hmeadi, M., Dyachok, O., Montaser, H., Lund, P.E., Yang, M., Ibrahim, H*., et al.* (2022). Functional, metabolic and transcriptional maturation of human pancreatic islets derived from stem cells. Nat Biotechnol *40*, 1042-1055.

Barros, C.S., Franco, S.J., and Muller, U. (2011). Extracellular matrix: functions in the nervous system. Cold Spring Harb Perspect Biol *3*, a005108.

Bastidas-Ponce, A., Tritschler, S., Dony, L., Scheibner, K., Tarquis-Medina, M., Salinno, C., Schirge, S., Burtscher, I., Bottcher, A., Theis, F.J*., et al.* (2019). Comprehensive single cell mRNA profiling reveals a detailed roadmap for pancreatic endocrinogenesis. Development *146*.

Bechard, M.E., Bankaitis, E.D., Hipkens, S.B., Ustione, A., Piston, D.W., Yang, Y.P., Magnuson, M.A., and Wright, C.V. (2016). Precommitment low-level Neurog3 expression defines a long-lived mitotic endocrine-biased progenitor pool that drives production of endocrine-committed cells. Genes Dev *30*, 1852-1865.

Berglund, E.D., Li, C.Y., Poffenberger, G., Ayala, J.E., Fueger, P.T., Willis, S.E., Jewell, M.M., Powers, A.C., and Wasserman, D.H. (2008). Glucose metabolism in vivo in four commonly used inbred mouse strains. Diabetes *57*, 1790-1799.

Blum, B., Roose, A.N., Barrandon, O., Maehr, R., Arvanites, A.C., Davidow, L.S., Davis, J.C., Peterson, Q.P., Rubin, L.L., and Melton, D.A. (2014). Reversal of beta cell de-differentiation by a small molecule inhibitor of the TGFbeta pathway. Elife *3*, e02809.

Bolger, A.M., Lohse, M., and Usadel, B. (2014). Trimmomatic: a flexible trimmer for Illumina sequence data. Bioinformatics *30*, 2114-2120.

Campbell, J.E., and Newgard, C.B. (2021). Mechanisms controlling pancreatic islet cell function in insulin secretion. Nat Rev Mol Cell Biol *22*, 142-158.

Carlson, T.R., Hu, H., Braren, R., Kim, Y.H., and Wang, R.A. (2008). Cell-autonomous requirement for beta1 integrin in endothelial cell adhesion, migration and survival during angiogenesis in mice. Development *135*, 2193-2202.

Chen, S., Zhou, Y., Chen, Y., and Gu, J. (2018). fastp: an ultra-fast all-in-one FASTQ preprocessor. Bioinformatics *34*, i884-i890.

Cirulli, V., Beattie, G.M., Klier, G., Ellisman, M., Ricordi, C., Quaranta, V., Frasier, F., Ishii, J.K., Hayek, A., and Salomon, D.R. (2000). Expression and function of alpha(v)beta(3) and alpha(v)beta(5) integrins in the developing pancreas: roles in the adhesion and migration of putative endocrine progenitor cells. J Cell Biol *150*, 1445-1460.

Cottle, L., Gan, W.J., Gilroy, I., Samra, J.S., Gill, A.J., Loudovaris, T., Thomas, H.E., Hawthorne, W.J., Kebede, M.A., and Thorn, P. (2021). Structural and functional polarisation of human

1239 pancreatic beta cells in islets from organ donors with and without type 2 diabetes. Diabetologia
1240 *64*, 618-629.
1241 Dahl, U., Sjodin, A., and Semb, H. (1996). Cadherins regulate aggregation of pancreatic beta-
1242 cells in vivo. Development *122*, 2895-2902.
1243 Diaferia, G.R., Jimenez-Caliani, A.J., Ranjitkar, P., Yang, W., Hardiman, G., Rhodes, C.J., Crisa,
1244 L., and Cirulli, V. (2013). beta1 integrin is a crucial regulator of pancreatic beta-cell expansion.
1245 Development *140*, 3360-3372.
1246 DiGruccio, M.R., Mawla, A.M., Donaldson, C.J., Noguchi, G.M., Vaughan, J., Cowing-Zitron, C.,
1247 van der Meulen, T., and Huising, M.O. (2016). Comprehensive alpha, beta and delta cell
1248 transcriptomes reveal that ghrelin selectively activates delta cells and promotes somatostatin
1249 release from pancreatic islets. Mol Metab *5*, 449-458.
1250 Dobin, A., Davis, C.A., Schlesinger, F., Drenkow, J., Zaleski, C., Jha, S., Batut, P., Chaisson, M.,
1251 and Gingeras, T.R. (2013). STAR: ultrafast universal RNA-seq aligner. Bioinformatics *29*, 15-21.
1252 Dybala, M.P., Butterfield, J.K., Hendren-Santiago, B.K., and Hara, M. (2020). Pancreatic Islets
1253 and Gestalt Principles. Diabetes *69*, 1864-1874.
1254 Elghazi, L., Gould, A.P., Weiss, A.J., Barker, D.J., Callaghan, J., Opland, D., Myers, M., Cras-
1255 Meneur, C., and Bernal-Mizrachi, E. (2012). Importance of beta-Catenin in glucose and energy
1256 homeostasis. Sci Rep *2*, 693.
1257 Esni, F., Taljedal, I.B., Perl, A.K., Cremer, H., Christofori, G., and Semb, H. (1999). Neural cell
1258 adhesion molecule (N-CAM) is required for cell type segregation and normal ultrastructure in
1259 pancreatic islets. J Cell Biol *144*, 325-337.
1260 Fagotto, F. (2014). The cellular basis of tissue separation. Development *141*, 3303-3318.
1261 Foty, R.A., and Steinberg, M.S. (2005). The differential adhesion hypothesis: a direct evaluation.
1262 Dev Biol *278*, 255-263.
1263 Gan, W.J., Do, O.H., Cottle, L., Ma, W., Kosobrodova, E., Cooper-White, J., Bilek, M., and Thorn,
1264 P. (2018). Local Integrin Activation in Pancreatic beta Cells Targets Insulin Secretion to the
1265 Vasculature. Cell Rep *24*, 2819-2826 e2813.
1266 Gilbert, J.M., Adams, M.T., Sharon, N., Jayaraaman, H., and Blum, B. (2020). Morphogenesis of
1267 the islets of Langerhans is guided by extra-endocrine Slit2/3 signals. Mol Cell Biol.
1268 Gonschior, H., Haucke, V., and Lehmann, M. (2020). Super-Resolution Imaging of Tight and
1269 Adherens Junctions: Challenges and Open Questions. Int J Mol Sci *21*.
1270 Gouzi, M., Kim, Y.H., Katsumoto, K., Johansson, K., and Grapin-Botton, A. (2011). Neurogenin3
1271 initiates stepwise delamination of differentiating endocrine cells during pancreas development.
1272 Dev Dyn *240*, 589-604.
1273 Gu, G., Dubauskaite, J., and Melton, D.A. (2002). Direct evidence for the pancreatic lineage:
1274 NGN3+ cells are islet progenitors and are distinct from duct progenitors. Development *129*, 2447-
1275 2457.
1276 Halban, P.A., Powers, S.L., George, K.L., and Bonner-Weir, S. (1987). Spontaneous
1277 reassociation of dispersed adult rat pancreatic islet cells into aggregates with three-dimensional
1278 architecture typical of native islets. Diabetes *36*, 783-790.
1279 Hannigan, G., Troussard, A.A., and Dedhar, S. (2005). Integrin-linked kinase: a cancer
1280 therapeutic target unique among its ILK. Nat Rev Cancer *5*, 51-63.
1281 Harris, J.A., Hirokawa, K.E., Sorensen, S.A., Gu, H., Mills, M., Ng, L.L., Bohn, P., Mortrud, M.,
1282 Ouellette, B., Kidney, J.*, et al.* (2014). Anatomical characterization of Cre driver mice for neural
1283 circuit mapping and manipulation. Front Neural Circuits *8*, 76.
1284 Heinis, M., Simon, M.T., Ilc, K., Mazure, N.M., Pouyssegur, J., Scharfmann, R., and Duvillie, B.
1285 (2010). Oxygen tension regulates pancreatic beta-cell differentiation through hypoxia-inducible
1286 factor 1alpha. Diabetes *59*, 662-669.
1287 Huang da, W., Sherman, B.T., and Lempicki, R.A. (2009a). Bioinformatics enrichment tools: paths
1288 toward the comprehensive functional analysis of large gene lists. Nucleic Acids Res *37*, 1-13.

1289 Huang da, W., Sherman, B.T., and Lempicki, R.A. (2009b). Systematic and integrative analysis
1290 of large gene lists using DAVID bioinformatics resources. Nat Protoc *4*, 44-57.
1291 Jamora, C., and Fuchs, E. (2002). Intercellular adhesion, signalling and the cytoskeleton. Nat Cell
1292 Biol *4*, E101-108.
1293 Jiang, L., Sun, J., and Huang, D. (2022). Role of Slit/Robo Signaling pathway in Bone Metabolism.
1294 Int J Biol Sci *18*, 1303-1312.
1295 Jimenez-Caliani, A.J., Pillich, R., Yang, W., Diaferia, G.R., Meda, P., Crisa, L., and Cirulli, V.
1296 (2017). alphaE-Catenin Is a Positive Regulator of Pancreatic Islet Cell Lineage Differentiation.
1297 Cell Rep *20*, 1295-1306.
1298 Jo, J., Kilimnik, G., Kim, A., Guo, C., Periwal, V., and Hara, M. (2011). Formation of pancreatic
1299 islets involves coordinated expansion of small islets and fission of large interconnected islet-like
1300 structures. Biophys J *101*, 565-574.
1301 Kim, A., Miller, K., Jo, J., Kilimnik, G., Wojcik, P., and Hara, M. (2009). Islet architecture: A
1302 comparative study. Islets *1*, 129-136.
1303 Kragl, M., Schubert, R., Karsjens, H., Otter, S., Bartosinska, B., Jeruschke, K., Weiss, J., Chen,
1304 C., Alsteens, D., Kuss, O*., et al.* (2016). The biomechanical properties of an epithelial tissue
1305 determine the location of its vasculature. Nat Commun *7*, 13560.
1306 Krishnamurthy, M., Li, J., Fellows, G.F., Rosenberg, L., Goodyer, C.G., and Wang, R. (2011).
1307 Integrin alpha3, but not beta1, regulates islet cell survival and function via PI3K/Akt signaling
1308 pathways. Endocrinology *152*, 424-435.
1309 Kwon, H.R., Nelson, D.A., DeSantis, K.A., Morrissey, J.M., and Larsen, M. (2017). Endothelial
1310 cell regulation of salivary gland epithelial patterning. Development *144*, 211-220.
1311 Lammert, E., Gu, G., McLaughlin, M., Brown, D., Brekken, R., Murtaugh, L.C., Gerber, H.P.,
1312 Ferrara, N., and Melton, D.A. (2003). Role of VEGF-A in vascularization of pancreatic islets. Curr
1313 Biol *13*, 1070-1074.
1314 Larsen, H.L., and Grapin-Botton, A. (2017). The molecular and morphogenetic basis of pancreas
1315 organogenesis. Semin Cell Dev Biol *66*, 51-68.
1316 Lemaire, K., Thorrez, L., and Schuit, F. (2016). Disallowed and Allowed Gene Expression: Two
1317 Faces of Mature Islet Beta Cells. Annu Rev Nutr *36*, 45-71.
1318 Li, J., Zhao, Z., Wang, J., Chen, G., Yang, J., and Luo, S. (2008). The role of extracellular matrix,
1319 integrins, and cytoskeleton in mechanotransduction of centrifugal loading. Mol Cell Biochem *309*,
1320 41-48.
1321 Liao, Y., Smyth, G.K., and Shi, W. (2019). The R package Rsubread is easier, faster, cheaper
1322 and better for alignment and quantification of RNA sequencing reads. Nucleic Acids Res *47*, e47.
1323 Lien, W.H., Klezovitch, O., Fernandez, T.E., Delrow, J., and Vasioukhin, V. (2006). alphaE-
1324 catenin controls cerebral cortical size by regulating the hedgehog signaling pathway. Science *311*,
1325 1609-1612.
1326 Maldonado, M., Serrill, J.D., and Shih, H.P. (2020). Painting the Pancreas in Three Dimensions:
1327 Whole-Mount Immunofluorescence Method. Methods Mol Biol *2155*, 193-200.
1328 Mohamed, T.H., Watanabe, H., Kaur, R., Belyea, B.C., Walker, P.D., Gomez, R.A., and Sequeira-
1329 Lopez, M.L.S. (2020). Renin-Expressing Cells Require beta1-Integrin for Survival and for
1330 Development and Maintenance of the Renal Vasculature. Hypertension *76*, 458-467.
1331 Mui, K.L., Chen, C.S., and Assoian, R.K. (2016). The mechanical regulation of integrin-cadherin
1332 crosstalk organizes cells, signaling and forces. J Cell Sci *129*, 1093-1100.
1333 Murtaugh, L.C., Law, A.C., Dor, Y., and Melton, D.A. (2005). Beta-catenin is essential for
1334 pancreatic acinar but not islet development. Development *132*, 4663-4674.
1335 Muzumdar, M.D., Tasic, B., Miyamichi, K., Li, L., and Luo, L. (2007). A global double-fluorescent
1336 Cre reporter mouse. Genesis *45*, 593-605.
1337 Nair, G.G., Liu, J.S., Russ, H.A., Tran, S., Saxton, M.S., Chen, R., Juang, C., Li, M.L., Nguyen,
1338 V.Q., Giacometti, S*., et al.* (2019). Recapitulating endocrine cell clustering in culture promotes
1339 maturation of human stem-cell-derived beta cells. Nat Cell Biol *21*, 263-274.

1340 Panzer, J.K., Cohrs, C.M., and Speier, S. (2020). Using Pancreas Tissue Slices for the Study of
1341 Islet Physiology. Methods Mol Biol *2128*, 301-312.
1342 Pauerstein, P.T., Tellez, K., Willmarth, K.B., Park, K.M., Hsueh, B., Efsun Arda, H., Gu, X.,
1343 Aghajanian, H., Deisseroth, K., Epstein, J.A.*, et al.* (2017). A radial axis defined by semaphorin-
1344 to-neuropilin signaling controls pancreatic islet morphogenesis. Development *144*, 3744-3754.
1345 Raghavan, S., Bauer, C., Mundschau, G., Li, Q., and Fuchs, E. (2000). Conditional ablation of
1346 beta1 integrin in skin. Severe defects in epidermal proliferation, basement membrane formation,
1347 and hair follicle invagination. J Cell Biol *150*, 1149-1160.
1348 Reinert, R.B., Cai, Q., Hong, J.Y., Plank, J.L., Aamodt, K., Prasad, N., Aramandla, R., Dai, C.,
1349 Levy, S.E., Pozzi, A.*, et al.* (2014). Vascular endothelial growth factor coordinates islet innervation
1350 via vascular scaffolding. Development *141*, 1480-1491.
1351 Robinson, M.D., McCarthy, D.J., and Smyth, G.K. (2010). edgeR: a Bioconductor package for
1352 differential expression analysis of digital gene expression data. Bioinformatics *26*, 139-140.
1353 Romer, A.I., and Sussel, L. (2015). Pancreatic islet cell development and regeneration. Curr Opin
1354 Endocrinol Diabetes Obes *22*, 255-264.
1355 Roscioni, S.S., Migliorini, A., Gegg, M., and Lickert, H. (2016). Impact of islet architecture on beta-
1356 cell heterogeneity, plasticity and function. Nat Rev Endocrinol *12*, 695-709.
1357 Rosenberg, L.C., Lafon, M.L., Pedersen, J.K., Yassin, H., Jensen, J.N., Serup, P., and Hecksher-
1358 Sorensen, J. (2010). The transcriptional activity of Neurog3 affects migration and differentiation
1359 of ectopic endocrine cells in chicken endoderm. Dev Dyn *239*, 1950-1966.
1360 Rulifson, I.C., Karnik, S.K., Heiser, P.W., ten Berge, D., Chen, H., Gu, X., Taketo, M.M., Nusse,
1361 R., Hebrok, M., and Kim, S.K. (2007). Wnt signaling regulates pancreatic beta cell proliferation.
1362 Proc Natl Acad Sci U S A *104*, 6247-6252.
1363 Sakai, T., Larsen, M., and Yamada, K.M. (2003). Fibronectin requirement in branching
1364 morphogenesis. Nature *423*, 876-881.
1365 Scheppke, L., Murphy, E.A., Zarpellon, A., Hofmann, J.J., Merkulova, A., Shields, D.J., Weis, S.M.,
1366 Byzova, T.V., Ruggeri, Z.M., Iruela-Arispe, M.L.*, et al.* (2012). Notch promotes vascular
1367 maturation by inducing integrin-mediated smooth muscle cell adhesion to the endothelial
1368 basement membrane. Blood *119*, 2149-2158.
1369 Schiesser, J.V., Loudovaris, T., Thomas, H.E., Elefanty, A.G., and Stanley, E.G. (2021). Integrin
1370 alphavbeta5 heterodimer is a specific marker of human pancreatic beta cells. Sci Rep *11*, 8315.
1371 Schonhoff, S.E., Giel-Moloney, M., and Leiter, A.B. (2004). Neurogenin 3-expressing progenitor
1372 cells in the gastrointestinal tract differentiate into both endocrine and non-endocrine cell types.
1373 Dev Biol *270*, 443-454.
1374 Scully, K.M., Skowronska-Krawczyk, D., Krawczyk, M., Merkurjev, D., Taylor, H., Livolsi, A.,
1375 Tollkuhn, J., Stan, R.V., and Rosenfeld, M.G. (2016). Epithelial cell integrin beta1 is required for
1376 developmental angiogenesis in the pituitary gland. Proc Natl Acad Sci U S A *113*, 13408-13413.
1377 Seymour, P.A., Bennett, W.R., and Slack, J.M. (2004). Fission of pancreatic islets during
1378 postnatal growth of the mouse. J Anat *204*, 103-116.
1379 Sharon, N., Chawla, R., Mueller, J., Vanderhooft, J., Whitehorn, L.J., Rosenthal, B., Gurtler, M.,
1380 Estanboulieh, R.R., Shvartsman, D., Gifford, D.K.*, et al.* (2019a). A Peninsular Structure
1381 Coordinates Asynchronous Differentiation with Morphogenesis to Generate Pancreatic Islets. Cell
1382 *176*, 790-804 e713.
1383 Sharon, N., Vanderhooft, J., Straubhaar, J., Mueller, J., Chawla, R., Zhou, Q., Engquist, E.N.,
1384 Trapnell, C., Gifford, D.K., and Melton, D.A. (2019b). Wnt Signaling Separates the Progenitor and
1385 Endocrine Compartments during Pancreas Development. Cell Rep *27*, 2281-2291 e2285.
1386 Shih, H.P., Gross, M.K., and Kioussi, C. (2007). Cranial muscle defects of Pitx2 mutants result
1387 from specification defects in the first branchial arch. Proc Natl Acad Sci U S A *104*, 5907-5912.
1388 Shih, H.P., Panlasigui, D., Cirulli, V., and Sander, M. (2016). ECM Signaling Regulates Collective
1389 Cellular Dynamics to Control Pancreas Branching Morphogenesis. Cell Rep *14*, 169-179.

Shih, H.P., and Sander, M. (2014). Pancreas development ex vivo: culturing embryonic pancreas explants on permeable culture inserts, with fibronectin-coated glass microwells, or embedded in three-dimensional Matrigel. Methods Mol Biol *1210*, 229-237.

Shih, H.P., Wang, A., and Sander, M. (2013). Pancreas organogenesis: from lineage determination to morphogenesis. Annu Rev Cell Dev Biol *29*, 81-105.

Shiota, C., Prasadan, K., Guo, P., Fusco, J., Xiao, X., and Gittes, G.K. (2017). Gcg (CreERT2) knockin mice as a tool for genetic manipulation in pancreatic alpha cells. Diabetologia *60*, 2399-2408.

Simon-Areces, J., Membrive, G., Garcia-Fernandez, C., Garcia-Segura, L.M., and Arevalo, M.A. (2010). Neurogenin 3 cellular and subcellular localization in the developing and adult hippocampus. J Comp Neurol *518*, 1814-1824.

Speicher, T., Siegenthaler, B., Bogorad, R.L., Ruppert, R., Petzold, T., Padrissa-Altes, S., Bachofner, M., Anderson, D.G., Koteliansky, V., Fassler, R.*, et al.* (2014). Knockdown and knockout of beta1-integrin in hepatocytes impairs liver regeneration through inhibition of growth factor signalling. Nat Commun *5*, 3862.

Srinivas, S., Watanabe, T., Lin, C.S., William, C.M., Tanabe, Y., Jessell, T.M., and Costantini, F. (2001). Cre reporter strains produced by targeted insertion of EYFP and ECFP into the ROSA26 locus. BMC Dev Biol *1*, 4.

Stine, R.R., Greenspan, L.J., Ramachandran, K.V., and Matunis, E.L. (2014). Coordinate regulation of stem cell competition by Slit-Robo and JAK-STAT signaling in the Drosophila testis. PLoS Genet *10*, e1004713.

Subramanian, A., Tamayo, P., Mootha, V.K., Mukherjee, S., Ebert, B.L., Gillette, M.A., Paulovich, A., Pomeroy, S.L., Golub, T.R., Lander, E.S.*, et al.* (2005). Gene set enrichment analysis: a knowledge-based approach for interpreting genome-wide expression profiles. Proc Natl Acad Sci U S A *102*, 15545-15550.

Sznurkowska, M.K., Hannezo, E., Azzarelli, R., Chatzeli, L., Ikeda, T., Yoshida, S., Philpott, A., and Simons, B.D. (2020). Tracing the cellular basis of islet specification in mouse pancreas. Nat Commun *11*, 5037.

T.J. Deerinck, E.B., A. Thor, M.H. Ellisman (2010). NCMIR Methods for 3D EM: A New Protocol for Preparation of Biological Specimens for Serial Block Face Scanning Electron Microscopy. In National Center for Microscopy and Imaging Research, University of California, San Diego

Taylor, B.L., Liu, F.F., and Sander, M. (2013). Nkx6.1 is essential for maintaining the functional state of pancreatic beta cells. Cell Rep *4*, 1262-1275.

Thorens, B., Tarussio, D., Maestro, M.A., Rovira, M., Heikkila, E., and Ferrer, J. (2015). Ins1(Cre) knock-in mice for beta cell-specific gene recombination. Diabetologia *58*, 558-565.

Tong, M., Jun, T., Nie, Y., Hao, J., and Fan, D. (2019). The Role of the Slit/Robo Signaling Pathway. J Cancer *10*, 2694-2705.

van der Meulen, T., and Huising, M.O. (2014). Maturation of stem cell-derived beta-cells guided by the expression of urocortin 3. Rev Diabet Stud *11*, 115-132.

van der Meulen, T., Mawla, A.M., DiGruccio, M.R., Adams, M.W., Nies, V., Dolleman, S., Liu, S., Ackermann, A.M., Caceres, E., Hunter, A.E.*, et al.* (2017). Virgin Beta Cells Persist throughout Life at a Neogenic Niche within Pancreatic Islets. Cell Metab *25*, 911-926 e916.

Vasioukhin, V., Bauer, C., Degenstein, L., Wise, B., and Fuchs, E. (2001). Hyperproliferation and defects in epithelial polarity upon conditional ablation of alpha-catenin in skin. Cell *104*, 605-617.

Wakae-Takada, N., Xuan, S., Watanabe, K., Meda, P., and Leibel, R.L. (2013). Molecular basis for the regulation of islet beta cell mass in mice: the role of E-cadherin. Diabetologia *56*, 856-866.

Wang, S., Matsumoto, K., Lish, S.R., Cartagena-Rivera, A.X., and Yamada, K.M. (2021). Budding epithelial morphogenesis driven by cell-matrix versus cell-cell adhesion. Cell *184*, 3702-3716 e3730.

Wang, S., Sekiguchi, R., Daley, W.P., and Yamada, K.M. (2017). Patterned cell and matrix dynamics in branching morphogenesis. J Cell Biol *216*, 559-570.

1441 Weber, G.F., Bjerke, M.A., and DeSimone, D.W. (2011). Integrins and cadherins join forces to
1442 form adhesive networks. J Cell Sci *124*, 1183-1193.
1443 Win, P.W., Oakie, A., Li, J., and Wang, R. (2020). Beta-cell beta1 integrin deficiency affects in
1444 utero development of islet growth and vascularization. Cell Tissue Res *381*, 163-175.
1445 Yamamoto, H., Ehling, M., Kato, K., Kanai, K., van Lessen, M., Frye, M., Zeuschner, D.,
1446 Nakayama, M., Vestweber, D., and Adams, R.H. (2015). Integrin beta1 controls VE-cadherin
1447 localization and blood vessel stability. Nat Commun *6*, 6429.
1448 Yashpal, N.K., Li, J., Wheeler, M.B., and Wang, R. (2005). Expression of beta1 integrin receptors
1449 during rat pancreas development--sites and dynamics. Endocrinology *146*, 1798-1807.
1450 Zeng, C., Mulas, F., Sui, Y., Guan, T., Miller, N., Tan, Y., Liu, F., Jin, W., Carrano, A.C., Huising,
1451 M.O.*, et al.* (2017). Pseudotemporal Ordering of Single Cells Reveals Metabolic Control of
1452 Postnatal beta Cell Proliferation. Cell Metab *25*, 1160-1175 e1111.
1453